Tetraspanin Tspan15 is an essential subunit of an ADAM10 scissor complex

Chek Ziu Koo[1,2]*, Neale Harrison[1]*, Peter J. Noy[1]*, Justyna Szyroka[1], Alexandra L. Matthews[1], Hung-En Hsia[3], Stephan A. Mueller[3], Johanna Tüshaus[3], Joelle Goulding[2,4], Katie Willis[1], Clara Apicella[1], Bethany Cragoe[1], Edward Davis[1], Murat Keles[1], Antonia Malinova[1], Thomas A. McFarlane[1], Philip R. Morrison[1], Michael C. Sykes[1], Haroon Ahmed[1], Alessandro Di Maio[1], Lisa Seipold[5], Paul Saftig[5], Eleanor Cull[1], Eric Rubinstein[6], Natalie S. Poulter[2,7], Stephen J. Briddon[2,4], Nicholas D. Holliday[4], Stefan F. Lichtenthaler[3] and Michael G. Tomlinson[1,2,#]

1School of Biosciences, University of Birmingham, Birmingham, United Kingdom. 2Centre of Membrane Proteins and Receptors (COMPARE), Universities of Birmingham and Nottingham, Midlands, United Kingdom; 3German Center for Neurodegenerative Diseases (DZNE) Munich, Neuroproteomics, Klinikum rechts der Isar, Technical University Munich and Munich Cluster for Systems Neurology (SyNergy), Munich, Germany; 4Division of Physiology, Pharmacology and Neuroscience, School of Life Sciences, University of Nottingham, Nottingham, United Kingdom; 5Institute of Biochemistry, Christian Albrechts University Kiel, Kiel, Germany; 6Inserm, U935, F-94807, Villejuif, France; 7Institute of Cardiovascular Sciences, University of Birmingham, Birmingham, United Kingdom.

*Authors contributed equally to this work.

#To whom correspondence should be addressed: Michael G. Tomlinson: School of Biosciences, College of Life and Environmental Sciences, University of Birmingham, Birmingham, B15 2TT, United Kingdom; E-mail: m.g.tomlinson@bham.ac.uk; Tel.: 44-(0)121-414-2507; Fax: 44-(0)121-414-5925.

Abstract

A disintegrin and metalloprotease 10 (ADAM10) is essential for embryonic development and impacts on diseases such as cancer, Alzheimer's and inflammatory diseases. ADAM10 is a 'molecular scissor' that proteolytically cleaves the extracellular region from over 100 substrates, including Notch, amyloid precursor protein, cadherins, growth factors and chemokines. ADAM10 was recently proposed to function as six distinct scissors with different substrates, depending on its association with one of six regulatory tetraspanins, termed TspanC8s. However, it remains unclear to what degree ADAM10 function is critically dependent on a TspanC8 partner. To address this, we generated the first monoclonal antibodies to Tspan15 as a model TspanC8. These were used to show that ADAM10 is the principal Tspan15-interacting protein, that Tspan15 expression requires ADAM10 in cell lines and primary cells, and that a synthetic ADAM10/Tspan15 fusion protein is a functional scissor. Together these findings suggest that ADAM10 exists as an intimate ADAM10/TspanC8 scissor complex.

15   **Introduction**

16   A disintegrin and metalloproteinase 10 (ADAM10) is a ubiquitously-expressed transmembrane

17   protein which acts as a 'molecular scissor' by cleaving the extracellular region from over 100

18   substrates, a process termed ectodomain shedding (Lichtenthaler *et al.* 2018). ADAM10 is

19   essential for embryonic development by activating Notch proteins which determine cell fate.

20   Other substrates include cadherin adhesion molecules, amyloid precursor protein, and

21   transmembrane growth factors and chemokines. As such, ADAM10 is important for health and

22   in diseases such as cancer, Alzheimer's and inflammatory diseases (Wetzel *et al.* 2017).

23   The tetraspanins are a superfamily of 33 transmembrane proteins in mammals which interact

24   with specific transmembrane partner proteins and regulate their intracellular trafficking, lateral

25   mobility and clustering at the cell surface (Termini and Gillette 2017; van Deventer *et al.* 2017).

26   The first crystal structure of a tetraspanin suggests the capacity for conformational change,

27   regulated by cholesterol binding within a cavity formed by the four transmembrane helices

28   (Zimmerman *et al.* 2016). This raises the possibility that tetraspanins regulate their partner

29   proteins as molecular switches. We and others have identified six TspanC8 tetraspanins as

30   regulators of ADAM10 intracellular trafficking and enzymatic maturation (Dornier *et al.* 2012;

31   Haining *et al.* 2012; Prox *et al.* 2012). The TspanC8s comprise Tspan5, 10, 14, 15, 17 and 33,

32   and are so-called because of eight cysteines within their large extracellular loop. Different cell

33   types express distinct TspanC8 repertoires (Matthews *et al.* 2017; Matthews *et al.* 2018) and

34   emerging evidence suggests that each TspanC8 may cause ADAM10 to cleave specific

35   substrates (Dornier *et al.* 2012; Jouannet *et al.* 2016; Noy *et al.* 2016; Reyat *et al.* 2017; Saint-

36   Pol *et al.* 2017; Seipold *et al.* 2018; Brummer *et al.* 2019). However, there is an urgent need to

37   generate monoclonal antibodies (mAbs) to all TspanC8s, to define fully their expression profiles

38   and functional mechanisms. Moreover, it remains to be determined whether ADAM10 functions

39   as an intimate ADAM10/TspanC8 complex or whether TspanC8s are merely modulators of

40   ADAM10 trafficking.

41   This study focuses on Tspan15 as a model TspanC8. Tspan15 is best characterised by its

42   capacity to promote ADAM10 cleavage of N-cadherin in cell lines and *in vivo* (Prox *et al.* 2012;

43   Jouannet *et al.* 2016; Noy *et al.* 2016; Seipold *et al.* 2018). Tspan15 is also upregulated, and is a

44   marker of poor prognosis, in certain cancers (Zhang *et al.* 2018; Hiroshima *et al.* 2019;

45   Sidahmed-Adrar *et al.* 2019) and promotes cancer progression in a mouse model (Zhang *et al.*

46   2018). The aims of this study were to generate the first Tspan15 mAbs and to test three

47   hypotheses that would support the theory that Tspan15 and ADAM10 exist together as a scissor

48   complex: first, that ADAM10 is the principal Tspan15-interacting protein; second, that Tspan15

49   expression requires ADAM10; and third, that covalently linking Tspan15 and ADAM10 together

50   as a single fusion protein yields a functional scissor.

51

3

Results

Generation of Tspan15 mAbs

The majority of anti-tetraspanin mAbs have epitopes within the large extracellular loop (LEL). However, it has been traditionally difficult to make mAbs to many tetraspanins due to lack of efficacy of recombinant LELs as immunogens. Furthermore, use of tetraspanins expressed in whole cells as the immunogen is complicated by their relatively high sequence conservation between species, their relatively small size and possible masking of mAb epitopes by larger partner proteins (Rubinstein *et al.* 2013). We therefore hypothesised that expression of human Tspan15 in ADAM10-knockout mouse cells would 'unmask' Tspan15, allowing the generation of a mAb response in mice immunised with these cells. Thus, ADAM10-knockout mouse embryonic fibroblasts (MEFs) (Reiss *et al.* 2005) stably overexpressing FLAG-tagged human Tspan15 were generated by lentiviral transduction, and cell lysates were immunoblotted with a FLAG antibody to confirm expression (Figure 1A). Immunisation of mice with these cells, and subsequent hybridoma generation, was outsourced to Abpro Therapeutics. Four positive hybridomas were identified by screening of hybridoma tissue culture supernatants by flow cytometry of wild-type versus CRISPR/Cas9 Tspan15-knockout Jurkat T cells (Figure 1B). The mAbs were isotyped as IgG1κ for clones 1C12, 4A4 and 5D4, and IgG2Bκ for 5F4 (data not shown). To investigate whether the Tspan15 mAbs might cross-react with other members of the TspanC8 family, HEK-293T cells were transfected with FLAG-tagged Tspan5, Tspan10, Tspan14, Tspan15, Tspan17 or Tspan33, and whole cell lysates western blotted. Tspan15 was detected by each of the four Tspan15 mAbs, but none of the other TspanC8s were detected (Figure 1C). To determine whether the Tspan15 mAbs can co-immunoprecipitate ADAM10, human platelets were lysed in the relatively stringent 1% digitonin lysis buffer that was previously used to identify TspanC8/ADAM10 interactions (Dornier *et al.* 2012; Haining *et al.* 2012). Tspan15 immunoprecipitation followed by ADAM10 western blotting showed that each mAb effectively co-immunoprecipitated ADAM10 (Figure 1D). Therefore, these data validate the four new mAbs as specific mouse anti-human Tspan15 reagents capable of immunoprecipitating Tspan15/ADAM10 complexes.
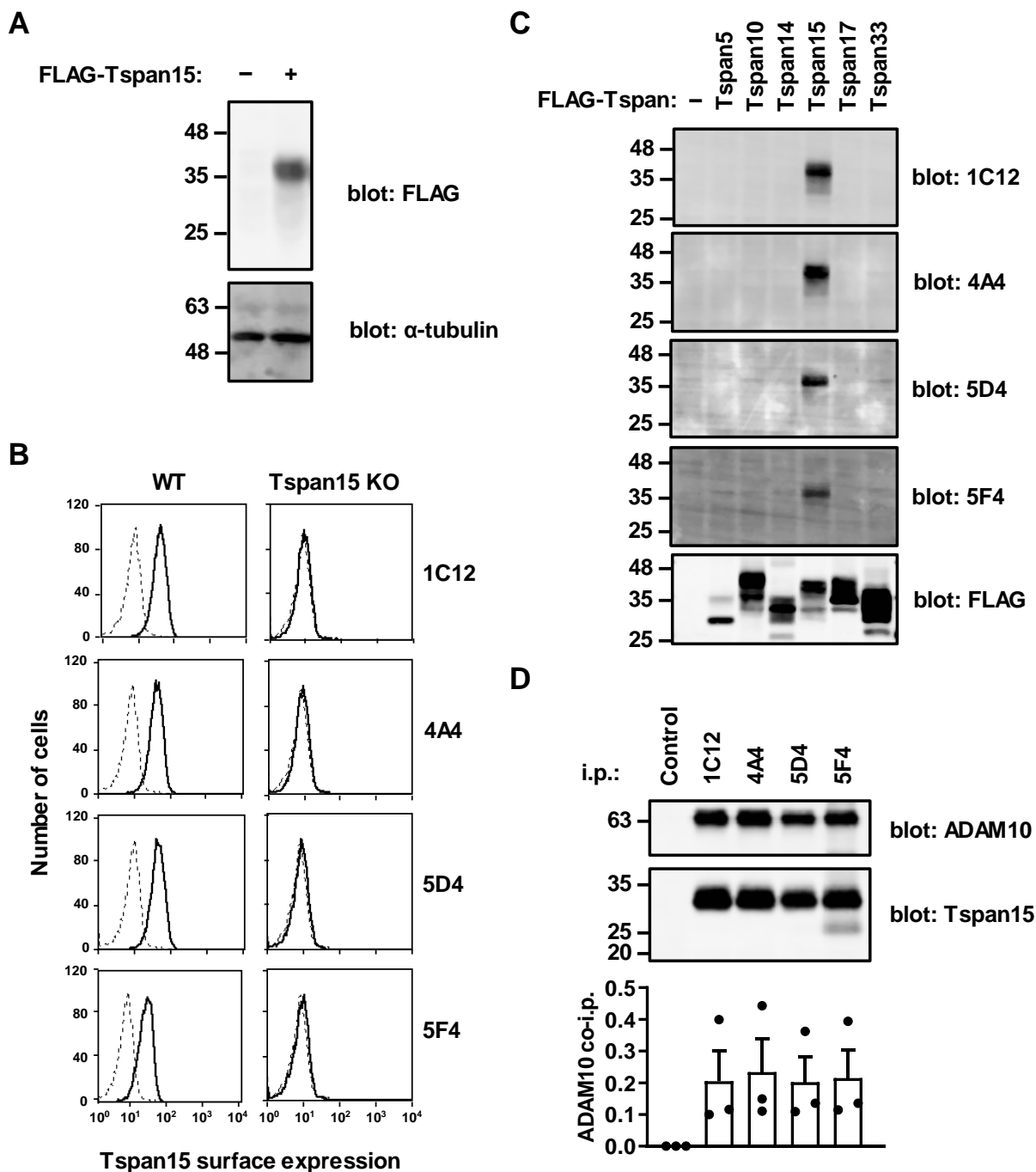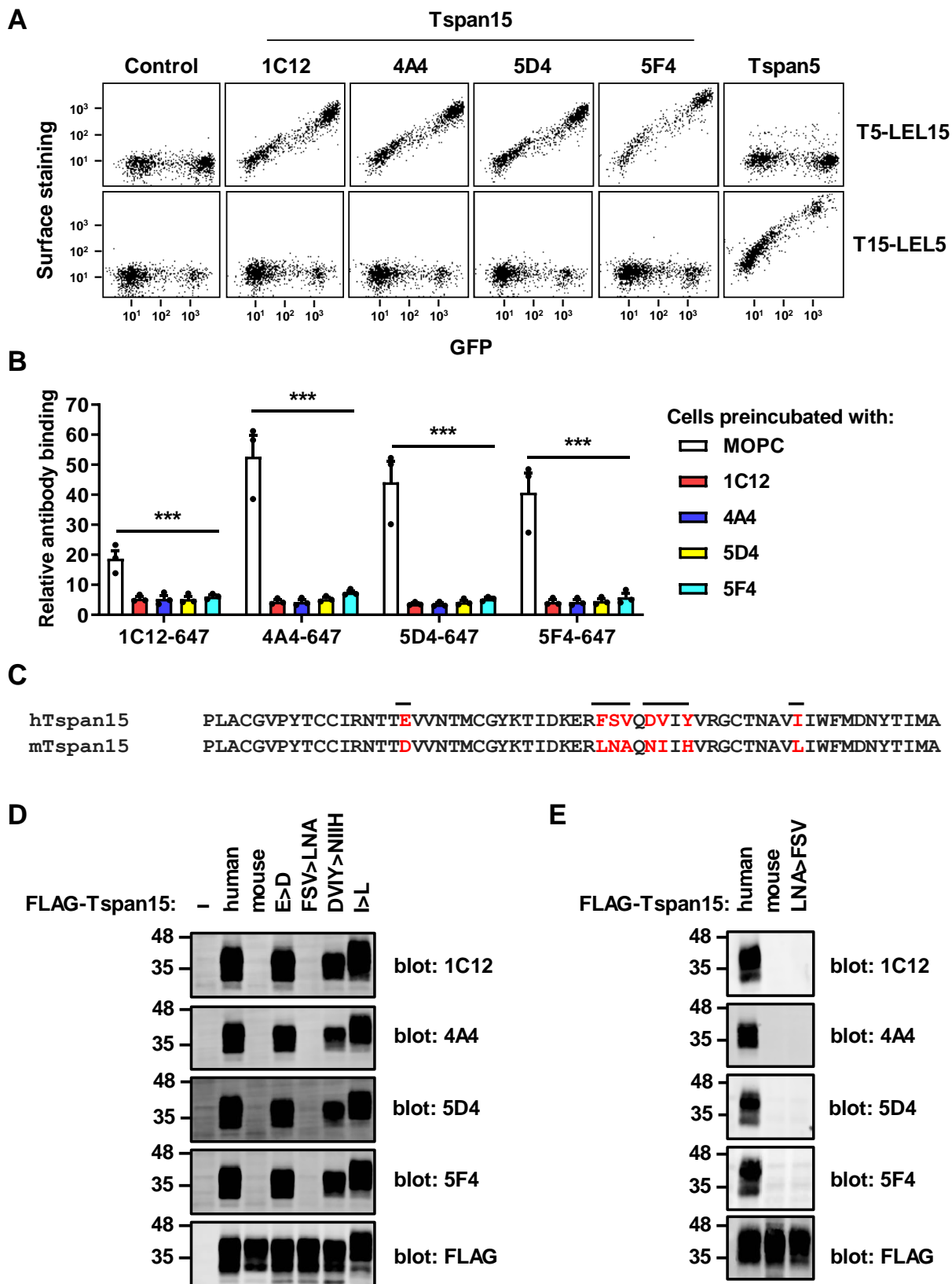
Figure 1. Generation of human Tspan15-expressing MEFs as an immunogen and validation of resulting mouse anti-human Tspan15 mAbs. (A) ADAM10-knockout MEFs (–) and ADAM10-knockout MEFs stably overexpressing FLAG-tagged Tspan15 (+) were lysed in 1% Triton X-100 lysis buffer and subjected to anti-FLAG (top panel) and anti-α-tubulin (bottom panel) western blotting. (B) Wild-type (WT) and Tspan15-knockout (KO) Jurkat human T cells

87   were analysed by flow cytometry with tissue culture supernatant for each of the four mouse anti-

88   human Tspan15 hybridomas (1C12, 4A4, 5D4 or 5F4; solid line), or with mouse IgG1 as a

89   negative control (dotted line). Histograms are representative of two independent experiments.

90   (C) HEK-293T cells were transfected with FLAG-tagged human TspanC8 expression constructs

91   (except for Tspan10, which was of mouse origin) or an empty vector control (–), lysed in 1%

92   Triton X-100 lysis buffer and western blotted with tissue culture supernatants for each of the four

93   Tspan15 hybridomas, or a positive control FLAG antibody. Blots are representative of three

94   independent experiments. (D) Human platelets were lysed in 1% digitonin lysis buffer and

95   subjected to immunoprecipitation with the four Tspan15 mAbs or a negative control mouse

96   IgG1, followed by anti-ADAM10 and anti-Tspan15 (5D4) western blotting (upper panels). The

97   faint additional band in the 5F4 lane corresponds to light chain from the immunoprecipitating

98   mAb (data not shown). To quantitate the data, the amount of ADAM10 co-immunoprecipitated

99   was normalised to the amount of immunoprecipitated Tspan15 with each antibody (lower panel).

100   Error bars represent standard error of the mean from three independent experiments.

101

**The four Tspan15 mAbs bind to similar epitopes in the large extracellular loop**

To determine whether the Tspan15 mAbs have epitopes in the large extracellular loop (LEL), previously described Tspan15/Tspan5 chimeric GFP-tagged constructs were used in which the LELs were exchanged (Saint-Pol *et al.* 2017). In flow cytometry analyses of transfected HEK-293T cells, the four Tspan15 mAbs detected the Tspan15 LEL on a Tspan5 backbone (T5-LEL15), but not the reciprocal protein (T15-LEL5) (Figure 2A). As a control, a Tspan5 mAb detected Tspan5 LEL on a Tspan15 backbone (Figure 2A), as previously reported (Saint-Pol *et al.* 2017). To investigate whether the Tspan15 mAbs have overlapping epitopes, an antibody binding competition assay was performed. To do this, the A549 lung epithelial cell line was preincubated with one of the Tspan15 mAbs or a control antibody, and then incubated with Tspan15 mAbs conjugated to Alexa Fluor® 647. Flow cytometry analyses showed that all four unlabelled Tspan15 mAbs inhibited binding of the each of the four labelled Tspan15 mAbs (Figure 2B), suggesting that their epitopes are located in close proximity. Within the Tspan15 LEL, only eight of the 121 amino acid residues vary between mouse and human, all within the C-terminal half of the LEL (Figure 2C). Since none of the Tspan15 mAbs detected mouse Tspan15 by western blotting (Figure 2D), this suggested that some of the differing residues were important for antibody binding. To determine which were important, four FLAG-tagged Tspan15 human/mouse chimeric constructs were made by substituting residues within the LEL of human Tspan15 with the corresponding mouse residues (Figure 2C), an approach that we used previously to epitope map mAbs to tetraspanin CD53 (Tomlinson *et al.* 1993; Tomlinson *et al.* 1995). Western blotting of lysates from transfected Tspan15-knockout HEK-293T cells showed that reactivity of all four Tspan15 mAbs was almost completely lost by changing residues FSV to LNA, but unaffected in the three other chimeras (Figure 2D). However, the human FSV sequence was not sufficient for recognition, because introduction of these residues into mouse Tspan15 did not enable recognition by the four Tspan15 mAbs (Figure 2E). Taken together, these data show that all four Tspan15 mAbs bind to similar epitopes within the LEL.

7

A

B

C

```
                                       _                   _ _ __       _
hTspan15   PLACGVPYTCCIRNTTEVVNTMCGYKTIDKERFSVQDVIYVRGCTNAVIIWFMDNYTIMA
mTspan15   PLACGVPYTCCIRNTTDVVNTMCGYKTIDKERLNAQNIIHVRGCTNAVLIWFMDNYTIMA
```

D

E

128

8

129 **Figure 2. The four Tspan15 mAbs bind to similar epitopes in the large extracellular loop.**
130 (A) Tspan15-knockout HEK-293T cells were transfected with GFP-tagged Tspan5 with the large
131 extracellular loop of Tspan15 (T5-LEL15) or the reciprocal chimeric expression construct (T15-
132 LEL5). Cells were stained with the four Tspan15 mAbs (1C12, 4A4, 5D4 or 5F4), Tspan5 mAb
133 (TS5-2) or negative control mouse IgG1, followed by APC-conjugated anti-mouse antibody and
134 flow cytometry analyses. (B) A549 cells were preincubated with one of the four unlabelled
135 Tspan15 mAbs, or a negative control mouse IgG1, for 30 minutes and stained with Alexa Fluor®
136 647-conjugated Tspan15 mAbs. Antibody binding, relative to unstained cells, was quantitated
137 by flow cytometry. Data were log-transformed and statistically analysed by a two-way ANOVA
138 with Tukey's multiple comparisons test. Error bars represent the standard error of the mean from
139 three independent experiments (***$p<0.001$ for control compared to each of the mAb
140 preincubations). (C) Amino acid sequence alignment of the C-terminal half of human (h) and
141 mouse (m) Tspan15 large extracellular loop region with Clustal Omega (Sievers *et al.* 2011).
142 Sequence differences are in red, and sequences exchanged in the four mutant constructs are
143 indicated by horizontal lines above the line-up. (D) Tspan15-knockout HEK-293T cells were
144 transfected with FLAG-tagged human Tspan15, mouse Tspan15, four chimeric constructs with
145 human Tspan15 residues replaced by corresponding mouse residues, or an empty vector control
146 (−). Cells were lysed in 1% Triton X-100 lysis buffer and subjected to anti-Tspan15 or anti-
147 FLAG western blotting. (E) Tspan15-knockout HEK-293T cells were transfected with FLAG-
148 tagged human Tspan15, mouse Tspan15 or a chimeric construct comprising mouse Tspan15 with
149 three residues of the corresponding human sequence. Cell lysates were western blotted as
150 described in panel D. Data for panels D-E are each representative of three experiments, from
151 which quantitation demonstrated no significant detection of mouse Tspan15 or the FSV to LNA
152 and reciprocal chimera (data not shown).

9

ADAM10 is the principal Tspan15-interacting protein

The generation of Tspan15 mAbs enabled the first proteomic identification of interactors with endogenous Tspan15. To do this, Tspan15 mAb 1C12 was used to immunoprecipitate Tspan15 from wild-type HEK-293T cells lysed in the relatively stringent detergent 1% digitonin; Tspan15-knockout cells were used as a negative control. Subsequent mass spectrometry identification revealed 28 proteins that were significantly detected in wild-type versus Tspan15-knockout samples from five independent experiments (Table 1 and Supplementary Table 1). Expression of the entire dataset as a volcano plot illustrated how the most significant and differential protein identified was ADAM10 (Figure 3). Indeed, ADAM10 and Tspan15 were the only proteins above the false discovery threshold for these experiments (Figure 3). These data suggest that ADAM10 is the principal Tspan15-interacting protein in HEK-293T cells.

164

165
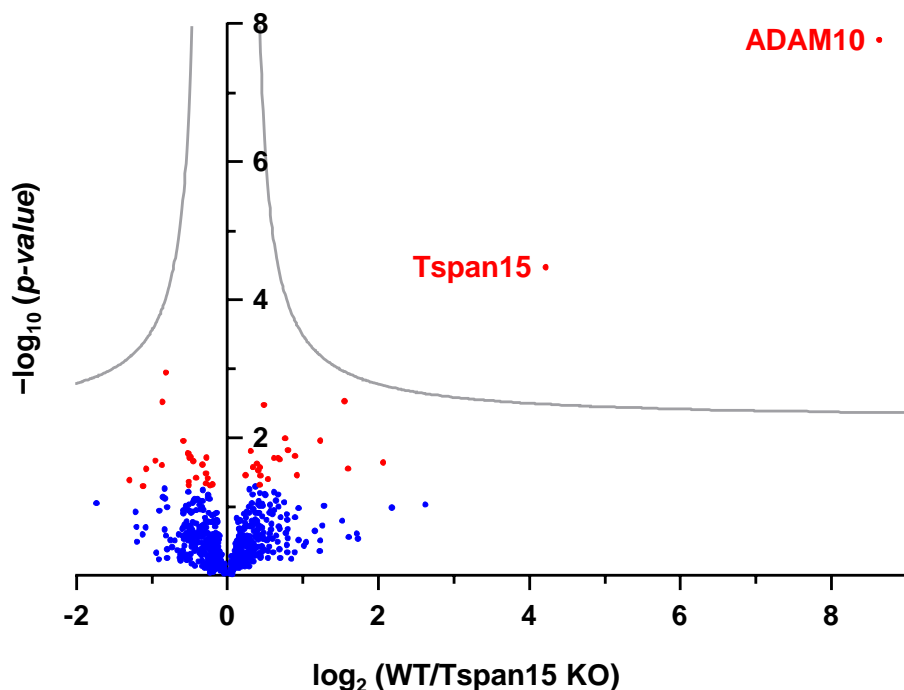
Figure 3. ADAM10 is the principal Tspan15-interacting protein in HEK-293T cells.
Wildtype (WT) and Tspan15-knockout (KO) HEK-293T cells were lysed in 1% digitonin lysis buffer and immunoprecipitated with Tspan15 mAb 1C12 cross-linked to protein G sepharose beads. Proteins were identified by liquid chromatography coupled with tandem mass spectrometry (LC-MS/MS). Proteomic profiles of WT and Tspan15 KO HEK-293T immunoprecipitates are presented in a volcano plot to identify differentially expressed proteins. The minus $\log_{10}$ transformed p-value of each protein was plotted against the $\log_2$ transformed protein label free quantification ratio between the Tspan15 co-immunoprecipitation of WT samples and the control co-immunoprecipitation of Tspan15 KO samples. Proteins with significant fold change ($p<0.05$) are depicted in red; blue dots represent proteins with no significant changes in expression. A permutation-based false discovery rate estimation was applied and visualised as hyperbolic curves in grey.

178

11

179 **Table 1. Proteins identified in Tspan15 immunoprecipitates.** The table contains proteins
180 significantly enriched in the Tspan15 immunoprecipitation samples of wild-type (WT) compared
181 to Tspan15-knockout (KO) samples. Five additional proteins detected in WT samples (in at least
182 3 of 5 biological replicates), but not in more than one Tspan15 KO sample, are indicated with an
183 asterisk. UniProt accession, protein name, gene name, *p*-value, fold difference between wild-
184 type and Tspan15-KO samples are listed. In addition, UniProt annotations indicate the
185 localization of the proteins.

186

Accession	Protein name	Gene name	*p*-value	Fold difference (WT vs KO)	Localization
O14672	Disintegrin and metalloproteinase domain-containing protein 10	ADAM10	1.70E-08	397.32	Membrane
O95858	Tetraspanin-15	TSPAN15	3.38E-05	18.57	Membrane
P52209	6-phosphogluconate dehydrogenase, decarboxylating	PGD	2.28E-02	4.18	Cytoplasm
P62879	Guanine nucleotide-binding protein G(I)/G(S)/G(T) subunit beta-2	GNB2	2.80E-02	3.02	Cytoplasm
Q08380	Galectin-3-binding protein	LGALS3BP	2.92E-03	2.92	x
Q14315	Filamin-C	FLNC	1.10E-02	2.34	Cytoplasm, Membrane
P46779	60S ribosomal protein L28	RPL28	3.47E-02	1.89	x
P27824	Calnexin	CANX	1.82E-02	1.86	Membrane
Q8WU90	Zinc finger CCCH domain-containing protein 15	ZC3H15	1.51E-02	1.75	Cytoplasm
Q8NEZ5	F-box only protein 22	FBXO22	1.02E-02	1.70	Cytoplasm
Q9HAD4	WD repeat-containing protein 41	WDR41	2.05E-02	1.61	Cytoplasm
Q12907	Vesicular integral-membrane protein VIP36	LMAN2	1.97E-02	1.59	Membrane
P63000	Ras-related C3 botulinum toxin substrate 1	RAC1	1.96E-02	1.53	Cytoplasm, Membrane
P23528	Cofilin-1	CFL1	3.95E-02	1.45	Cytoplasm, Membrane
Q4KMP7	TBC1 domain family member 10B	TBC1D10B	3.35E-03	1.40	Cytoplasm
Q9Y2G5	GDP-fucose protein O-fucosyltransferase 2	POFUT2	3.52E-02	1.35	x
P36639	7,8-dihydro-8-oxoguanine triphosphatase	NUDT1	2.69E-02	1.35	Cytoplasm
Q15020	Squamous cell carcinoma antigen recognized by T-cells 3	SART3	4.79E-02	1.34	Cytoplasm

12

| Q9P2E9	Ribosome-binding protein 1	RRBP1	2.95E-02	1.33	Membrane
Q13042	Cell division cycle protein 16 homolog	CDC16	2.39E-02	1.31	Cytoplasm
P27348	14-3-3 protein theta	YWHAQ	2.66E-02	1.27	Cytoplasm
Q8WUM4	Programmed cell death 6-interacting protein	PDCD6IP	1.56E-02	1.24	Cytoplasm
P40926	Malate dehydrogenase, mitochondrial	MDH2	3.49E-02	1.18	x
P62304	Small nuclear ribonucleoprotein E	SNRPE	*	0.73	Cytoplasm
O43172	U4/U6 small nuclear ribonucleoprotein Prp4	PRPF4	*	1.45	x
Q99878	Histone H2A type 1-J	HIST1H2AJ	*	0.73	x
P51809	Vesicle-associated membrane protein 7	VAMP7	*	1.88	Membrane
Q7L576	Cytoplasmic FMR1-interacting protein 1	CYFIP1	*	–	Cytoplasm

187

188

13

Tspan15 protein expression requires ADAM10

It is well established that TspanC8s promote the enzymatic maturation and trafficking of ADAM10 from the endoplasmic reticulum (ER) to the cell surface (Dornier *et al.* 2012; Haining *et al.* 2012; Prox *et al.* 2012). More recently, it was suggested that the reverse might be true, since ADAM10 knockdown reduced the trafficking of Tspan5 from the ER in HCT116 and U2OS cell lines (Saint-Pol *et al.* 2017). To investigate whether Tspan15 surface expression also requires ADAM10, flow cytometry was performed on CRISPR/Cas9 ADAM10-knockout cell lines. Tspan15 surface expression, as revealed by flow cytometry, was reduced by approximately 80% in the absence of ADAM10 in Jurkat, HEK-293T and A549 cells (Figure 4A). This observation held true in primary cells, since Tspan15 expression was almost undetectable following siRNA knockdown of ADAM10 in human umbilical vein endothelial cells (HUVECs) (Figure 4B). To determine whether the reduction in surface Tspan15 was consistent with a reduction in whole cell Tspan15, western blotting was performed on Tspan15 immunoprecipitates from Jurkat cell lysates. Similar to the flow cytometry data, Tspan15 protein expression was reduced by approximately 80% in the absence of ADAM10 (Figure 4C). Importantly, the loss of Tspan15 protein was not a consequence of reduced Tspan15 mRNA expression in the absence of ADAM10, as this was unaffected in ADAM10-knockout cell lines as measured by qRT-PCR (Figure 4D). These data demonstrate that ADAM10 and Tspan15 are each required for expression of the other, providing genetic evidence that the two proteins cooperate in a functional scissor complex.

The requirement of ADAM10 for normal Tspan15 protein expression is inconsistent with the fact that human Tspan15 was successfully expressed in ADAM10-knockout MEFs to generate the immunogen for Tspan15 mAb generation (Figure 1A). To address whether over-expression of Tspan15 might overcome the requirement for ADAM10, HEK-293T cells were transiently transfected with Tspan15 and analysed by flow cytometry. In this over-expression scenario, Tspan15 expression was comparable in wild-type versus ADAM10-knockout cells (Figure 4E). Therefore, it appears that endogenous Tspan15 protein expression requires ADAM10, but over-expressed Tspan15 can bypass this requirement.

14

217
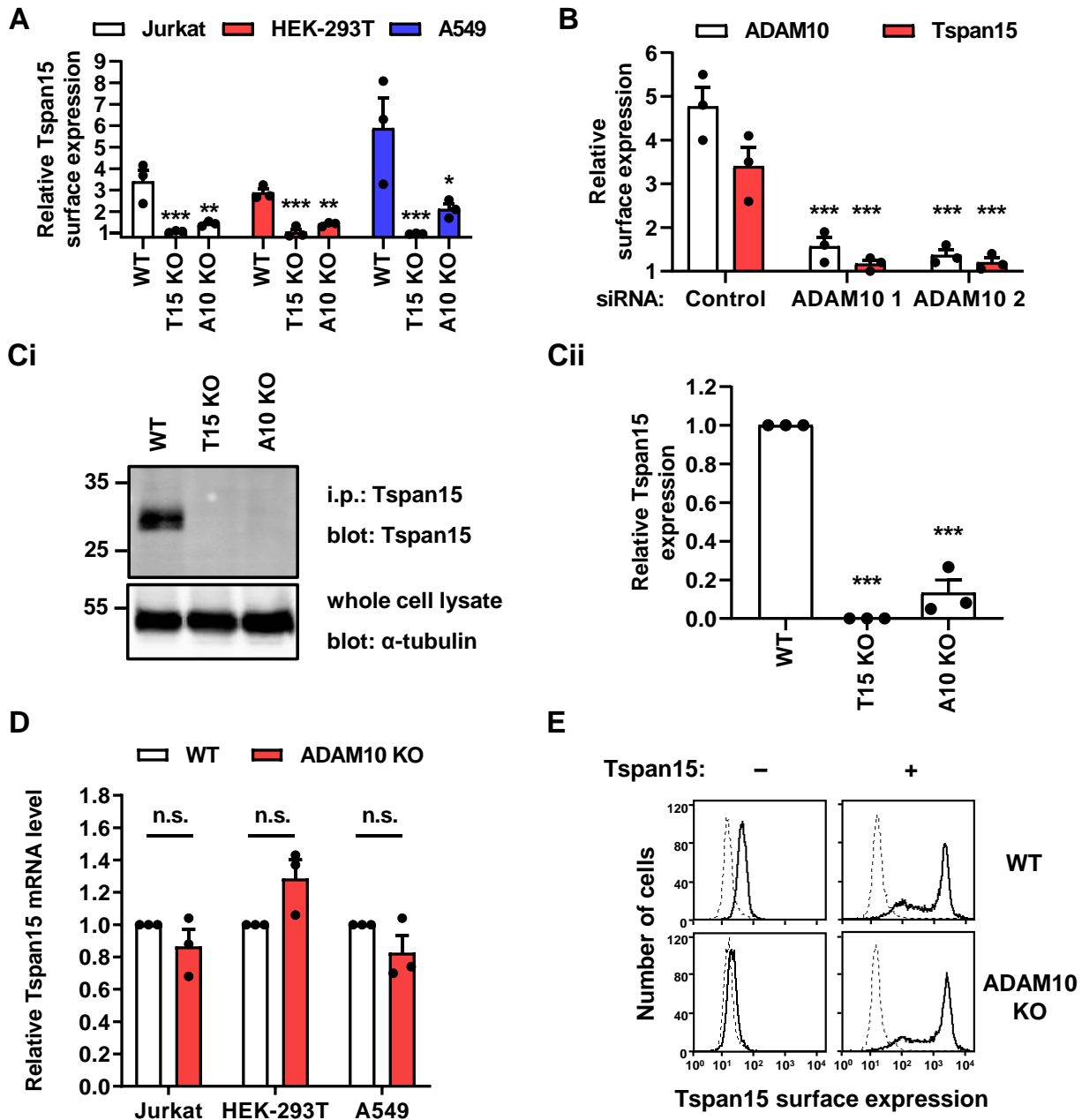
Figure 4. Tspan15 protein expression requires ADAM10. (A) Tspan15 surface expression in wildtype (WT), Tspan15-knockout (KO) and ADAM10 KO Jurkat, HEK-293T and A549 cell lines were analysed by flow cytometry with anti-Tspan15 mAb 1C12 or mouse IgG1 negative control antibody. Tspan15 surface expression is presented as the geometric mean fluorescence intensity of Tspan15 staining relative to the control staining. Error bars represent standard error of the mean from three independent experiments. Data were log-transformed and statistically analysed by a one-way ANOVA with Dunnett's multiple comparisons test (*$p<0.05$, **$p<0.01$, ***$p<0.001$ compared to WT). (B) HUVECs were transfected with two different ADAM10 siRNAs or a negative control siRNA and surface expression of ADAM10 and Tspan15 was

15

227   measured by flow cytometry and analysed as described in panel A. (Ci) WT, Tspan15 KO and

228   ADAM10 KO Jurkat cells were lysed in 1% Triton X-100 lysis buffer, immunoprecipitated with

229   anti-Tspan15 mAb 5D4, and western blotted with the same antibody. Whole cell lysates were

230   blotted with anti-α-tubulin mAb. (Cii) Tspan15 levels from panel Ci were quantitated and

231   normalised to WT expression. Error bars represent standard errors of the mean from three

232   independent experiments. Data were log-transformed and statistically analysed by a one-way

233   ANOVA with a Tukey's multiple comparisons test (***$p<0.001$ compared to WT). (D) Tspan15

234   mRNA level in WT and ADAM10 KO Jurkat, HEK-293T and A549 cells were assessed by qRT-

235   PCR and presented relative to GAPDH housekeeping gene expression. Error bars represent

236   standard errors of the mean from three independent experiments. Data were log-transformed and

237   statistically analysed by a two-way ANOVA followed by Tukey's multiple comparisons test

238   (n.s., not significant). (E) WT and ADAM10 KO HEK-293T cells were transfected with empty

239   vector control (−) or Tspan15 (+) expression constructs. Tspan15 surface expression was

240   measured by flow cytometry as described in panel A. Histograms are representative of four

241   independent experiments.

242

16

243 **The requirement of Tspan15 for ADAM10 surface expression is cell type dependent**

244 To assess the extent to which Tspan15 is required for ADAM10 surface expression in the cells

245 examined in Figure 4, flow cytometry for ADAM10 was performed. ADAM10 surface

246 expression was reduced by approximately 60% and 70% in Tspan15-knockout HEK-293T and

247 A549 cells, respectively, but was unaffected in Jurkat T cells (Figure 5A). In HUVECs,

248 ADAM10 surface expression was reduced by approximately 40% following Tspan15 siRNA

249 knockdown (Figure 5B). Therefore, the importance of Tspan15 for ADAM10 surface expression

250 depends on the cell type.

251

252

253
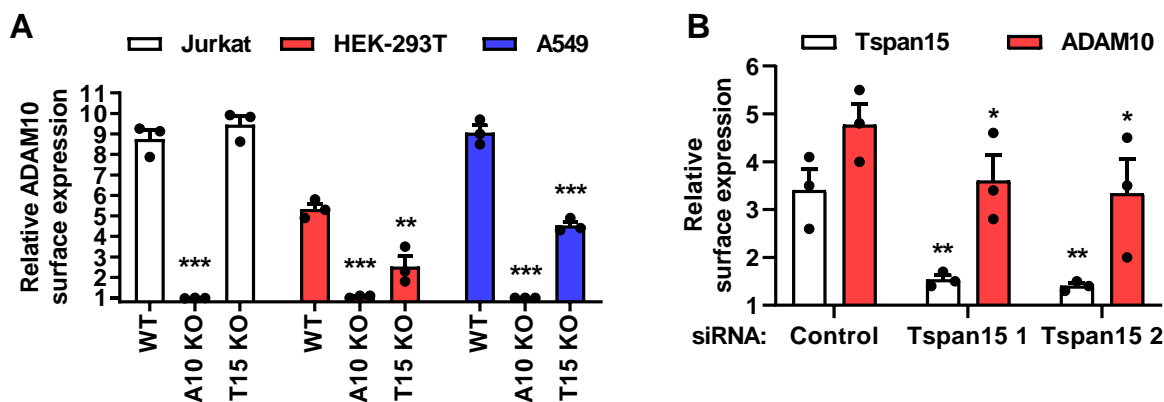
Figure 5. The requirement of Tspan15 for ADAM10 surface expression is cell type dependent. (A) ADAM10 surface expression in WT, ADAM10 KO and Tspan15 KO Jurkat, HEK-293T and A549 cells was measured by flow cytometry and quantitated as described in Figure 4A. (B) HUVECs were transfected with two different Tspan15 siRNAs or negative control siRNA and surface expression of ADAM10 was measured by flow cytometry and analysed as described in Figure 4A.

ADAM10 and Tspan15 form dynamic bimolecular fluorescence complementation (BiFC) complexes

A single particle tracking study has previously reported an apparent diffusion coefficient for ADAM10 of 0.067 μm^2/s in U2OS cells, which increased to 0.104 μm^2/s following Tspan15 transfection (Jouannet *et al.* 2016). To more directly assess the lateral diffusion of ADAM10/Tspan15 complexes, and to image an ADAM10/Tspan15 dimer for the first time, bimolecular fluorescence complementation (BiFC) was employed. This technique allows formation of fluorescent protein dimers from two interacting proteins tagged with split fluorescent proteins, in this case Tspan15 fused to the N-terminal half of superfolder (sf)GFP and ADAM10 fused to the C-terminal half of sfGFP (Figure 6A). Formation of fluorescent BiFC ADAM10/Tspan15 dimers was confirmed by confocal microscopy of transfected HEK-293T cells, which showed a BiFC signal predominantly at the cell surface, similar to Tspan15 itself (Figure 6B). To examine the lateral diffusion of ADAM10/Tspan15 dimers on the apical membrane of transfected HEK-293T cells, fluorescence correlation spectroscopy (FCS) was used. The average number of fluorescent complexes/μm^2 was 48 and the average diffusion speed was 0.19 μm^2/s (Figure 6C-D). To then provide an indication of the oligomerisation state of the molecules, the average molecular brightness of ADAM10/Tspan15 dimers was determined using photon counting histogram (PCH) analysis. Of the FCS traces analysed, 58% fitted to a one-component PCH model (molecular brightness of 2.2×10^4 cpm/s), whereas the remaining preferentially fitted to a two-component model that had dimmer (1.4×10^4 cpm/s) and brighter (5.4×10^4 cpm/s) subcomponents (Figure 6E). The molecular brightness of the dimmer traces was not significantly different from the one-component traces (Figure 6E). The presence of a brighter subcomponent suggests that some ADAM10/Tspan15 complexes were able to form larger clusters. Collectively, these data show that ADAM10 and Tspan15 can interact with each other to form dynamic BiFC dimers of varying stoichiometric ratio within nanoclusters.
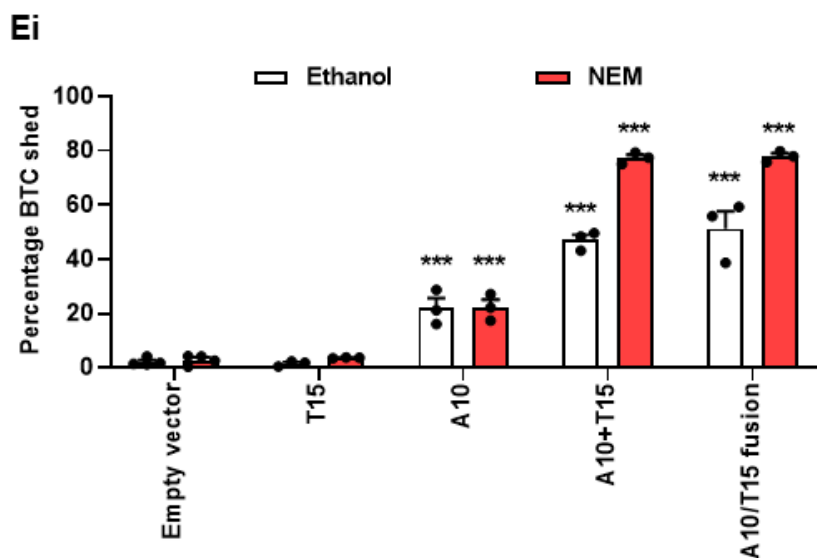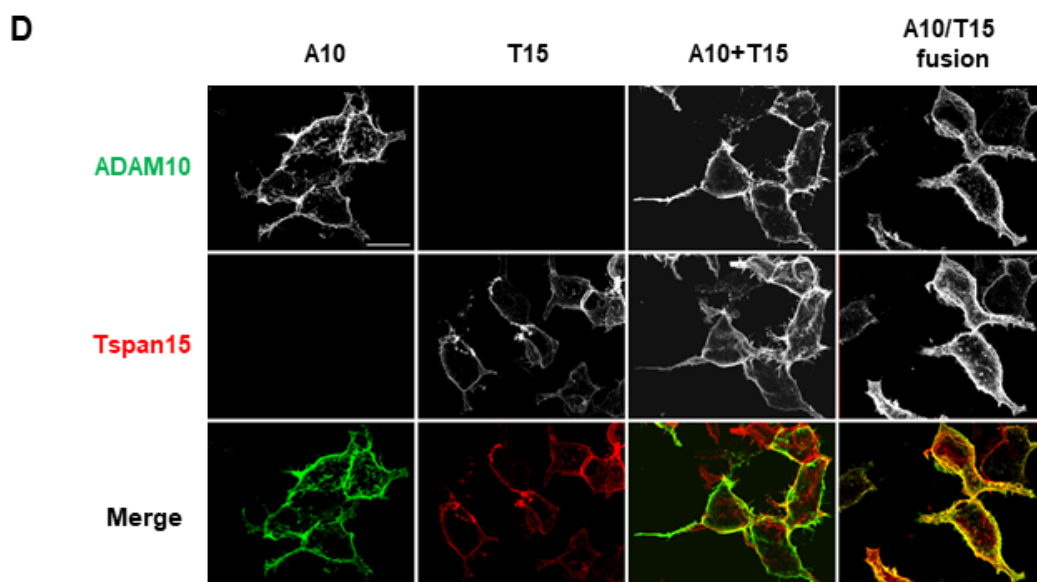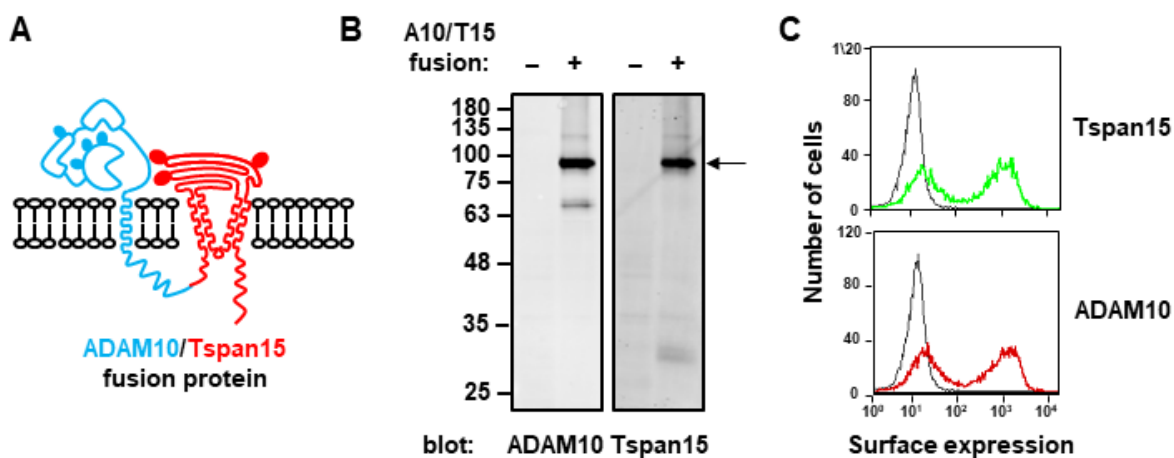
285
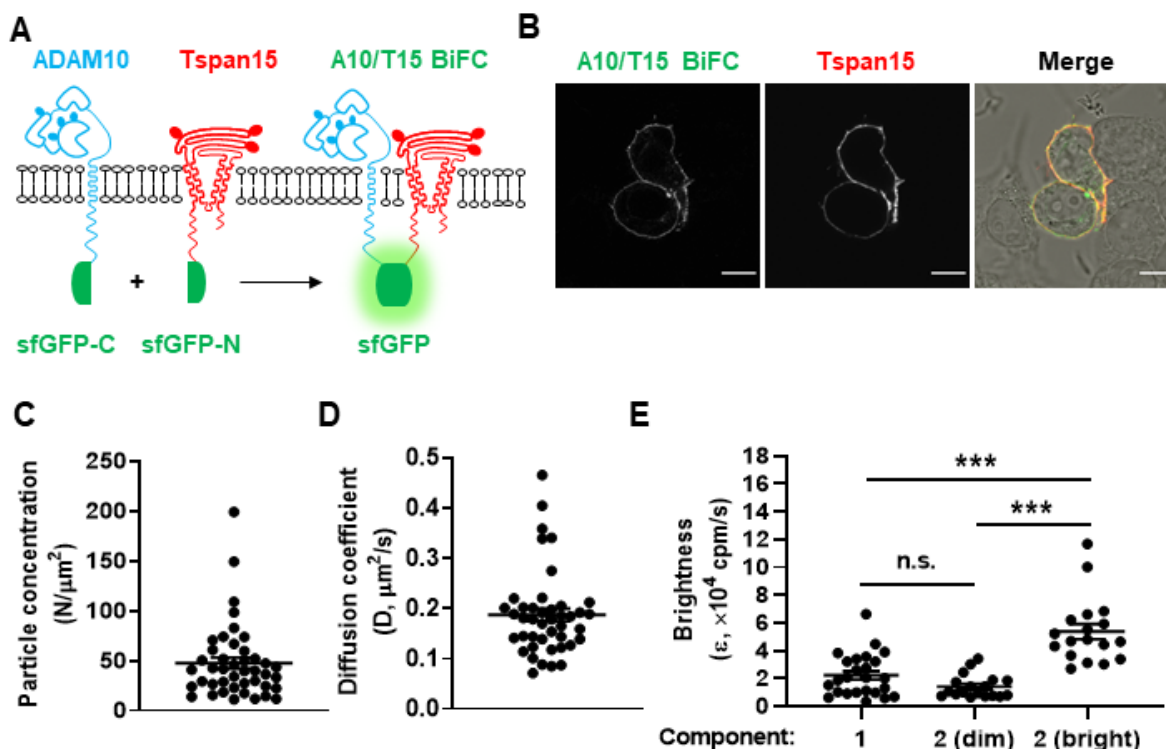
Figure 6. ADAM10 and Tspan15 form dynamic bimolecular fluorescence complementation (BiFC) complexes. (A) Schematic representation of ADAM10 tagged with the C-terminal half of superfolder GFP (sfGFP-C), Tspan15 tagged with the N-terminal half of superfolder GFP (sfGFP-N) and the predicted ADAM10/Tspan15 BiFC dimer. Solid ovals represent N-glycosylation. (B) HEK-293T cells were transfected with the ADAM10 and Tspan15 BiFC expression constructs, fixed and stained with Alexa Fluor® 647-conjugated Tspan15 mAb 5D4, and analysed by confocal microscopy. The image shown is representative of middle plane sections taken from two independent experiments (scale bar 10 µm). (C-D) Fluorescence correlation spectroscopy (FCS) measurements from the upper membrane of HEK-293T expressing the ADAM10/Tspan15 BiFC complexes were used to determine the average particle concentration (C) and diffusion co-efficient (D) of the complexes. (E) Fluorescence fluctuations from the FCS reads were also subjected to photon counting histogram (PCH) analysis to obtain the average molecular brightness (ε) of particles within the confocal volume. The FCS data were separated into groups that preferentially fit to a one-component or a two-component PCH model with dimmer and brighter subcomponents. Data were obtained from 43 individual measurements from three independent experiments. Error bars represent standard errors of the mean, N is the number of particles, and cpm is the counts per molecule. Data were log-transformed and statistically analysed by a one-way ANOVA followed by Tukey's multiple comparisons test (***$p<0.001$).

305

20

A synthetic ADAM10/Tspan15 fusion protein is a functional scissor

If ADAM10 and Tspan15 cooperate in a functional scissor complex, one prediction is that covalently linking the two proteins into one synthetic fusion protein (Figure 7A) would not disrupt subcellular localisation or scissor function. An ADAM10/Tspan15 fusion expression construct was generated and transfected into ADAM10/Tspan15 double knockout HEK-293T cells. Western blotting with ADAM10 and Tspan15 mAbs verified that the ADAM10/Tspan15 fusion protein had the predicted molecular weight of approximately 95 kD (Figure 7B), and flow cytometry (Figure 7C) and confocal microscopy (Figure 7D) showed that it was expressed at the cell surface. To test scissor function, ADAM10/Tspan15 double knockout HEK-293T cells were transfected with an expression construct for alkaline phosphatase-tagged betacellulin, a known ADAM10 substrate (Sahin *et al.* 2004), and shedding quantitated by measuring alkaline phosphatase activity released into the culture supernatant versus the non-shed activity remaining with the cells. Transfection of ADAM10/Tspan15 double knockout cells with the ADAM10/Tspan15 fusion protein construct restored betacellulin shedding to a level comparable to that of ADAM10 and Tspan15 transfected as individual constructs, in terms of both basal shedding and shedding induced by the ADAM10 activator N-ethylmaleimide (NEM) (Figure 7Ei). Betacellulin shedding was partially dependent on Tspan15, because ADAM10 transfection alone was not sufficient to fully restore shedding (Figure 7Ei). To confirm expression of the constructs used in these experiments, ADAM10 flow cytometry was used; the fusion protein was expressed at approximately two-fold greater levels than ADAM10 individually with Tspan15 (Figure 7Eii). These fusion protein data provide further evidence that ADAM10/Tspan15 exists as a functional scissor complex, because expression and function of the fusion protein are similar to when ADAM10 and Tspan15 are individually co-expressed.

A ADAM10/Tspan15 fusion protein

B A10/T15 fusion: − + − + ; blot: ADAM10 Tspan15

C Tspan15 / ADAM10 — Surface expression

D A10, T15, A10+T15, A10/T15 fusion — ADAM10, Tspan15, Merge

Ei Percentage BTC shed — Ethanol / NEM

Eii Relative ADAM10 surface expression

330

331 **Figure 7. A synthetic ADAM10/Tspan15 fusion protein is a functional scissor.** (A)

332 Schematic representation of the synthetic ADAM10/Tspan15 fusion protein that has the C-

333 terminus of ADAM10 physically linked to the N-terminus of Tspan15. Solid ovals represent N-

334 glycosylation. (B) ADAM10/Tspan15 double KO HEK-293T cells were transfected with

335 ADAM10/Tspan15 fusion construct, lysed in 1% digitonin lysis buffer in the presence of 10 µM

336 ADAM10 inhibitor GI254023X, to prevent post-lysis auto-proteolysis, and western blotted for

337 ADAM10 and Tspan15. (C) Cells described in panel B were assessed for surface expression of

338 Tspan15 (green) and ADAM10 (red) by flow cytometry. Black traces represent isotype control

339 staining. (D) ADAM10/Tspan15 double KO HEK-293T cells were transfected with the

340 indicated expression constructs and analysed by confocal microscopy using anti-ADAM10

341 (green) and Tspan15 (red) mAbs. The cells were non-permeabilised and images are maximum

342 intensity projections of confocal z-stacks. The scale bar on the upper left image is 30 µm. (Ei)

343 ADAM10/Tspan15 double KO HEK-293T cells were co-transfected with alkaline phosphatase-

344 tagged betacellulin (BTC) and Tspan15, ADAM10, ADAM10 and Tspan15, the

345 ADAM10/Tspan15 fusion, or an empty vector control. Cells were stimulated with 2 mM NEM

346 or vehicle control and alkaline phosphatase activity was measured in the supernatant and whole

347 cell lysates to quantitate the percentage of BTC shed. Data were arcsine-transformed and

348 statistically analysed with a two-way ANOVA followed by a Tukey's multiple comparisons test

349 (***$p<0.001$ compared to empty vector-transfected control). (Eii) Transfected cells were

350 assessed for surface expression of ADAM10 by flow cytometry and the data quantitated and

351 analysed using a paired t-test (*$p<0.05$).

352

23

DISCUSSION

353

354 This study reports the generation of the first mAbs to tetraspanin Tspan15, which is one of six

355 TspanC8 tetraspanins that regulate the molecular scissor ADAM10 (Matthews *et al.* 2017;

356 Matthews *et al.* 2017; Saint-Pol *et al.* 2017) and was recently shown to promote cancer (Zhang *et*

357 *al.* 2018). These mAbs enabled three major findings: (1) ADAM10 is the principal Tspan15-

358 interacting protein; (2) Tspan15 expression requires ADAM10; and (3) a synthetic

359 ADAM10/Tspan15 fusion protein is a functional scissor. These data strongly suggest that

360 ADAM10 and Tspan15 exist as a heterodimeric scissor complex.

361 The discovery that Tspan15 expression requires ADAM10 provides genetic evidence that the

362 principal role of Tspan15 is to regulate ADAM10. This finding is consistent with a recent study

363 on Tspan5 and ADAM10 (Saint-Pol *et al.* 2017). In that study, an approximate 70% siRNA

364 knockdown of ADAM10 in the HCT116 and U2OS cell lines reduced Tspan5 expression by

365 40%, and ADAM10 was shown to be important for trafficking of Tspan5 out of the ER (Saint-

366 Pol *et al.* 2017). In the current study, we were able to investigate Tspan15 expression in the

367 complete absence of ADAM10 by CRISPR/Cas9 knockout in three different cell lines, namely

368 A549, HEK-293T and Jurkat. In each ADAM10-knockout cell line, Tspan15 expression was

369 reduced by approximately 80%, as measured by flow cytometry and western blotting. Primary

370 HUVECs yielded similar data, since 85-90% ADAM10 knockdown resulted in an equivalent

371 reduction in Tspan15 protein expression. Importantly, Tspan15 mRNA expression levels were

372 unaffected by ADAM10 knockout, indicating a specific effect on Tspan15 protein. Thus,

373 Tspan15 and ADAM10 appear to be each required for the normal expression of the other.

374 Indeed, it is well established that TspanC8s are important for ADAM10 maturation and

375 trafficking to the cell surface (Dornier *et al.* 2012; Haining *et al.* 2012; Prox *et al.* 2012; Zhou *et*

376 *al.* 2014; Jouannet *et al.* 2016; Noy *et al.* 2016; Virreira Winter *et al.* 2016; Reyat *et al.* 2017;

377 Brummer *et al.* 2018; Seipold *et al.* 2018; Shah *et al.* 2018; Brummer *et al.* 2019), and we

378 extended these observations by showing that ADAM10 surface expression was partially reduced

379 in the absence of Tspan15 in A549, HEK-293T and HUVECs. Expression of other TspanC8s by

380 these cells (Haining *et al.* 2012; Matthews *et al.* 2017) is likely to be the reason that the reduction

381 is only partial. However, the effect of Tspan15 on ADAM10 expression is cell type dependent,

382 because no ADAM10 reduction was observed in Tspan15-knockout Jurkat T cells. It remains

383 unclear why this is the case, but it is possible that Tspan15 protein expression is low in these

384 cells, relative to other tetraspanins.

385 The previously discussed finding that Tspan15 expression requires ADAM10 suggests that the

386 two proteins might exist as a functional complex. A prediction of this idea is that physically

387 linking the two proteins into a single fusion protein would yield a functional scissor protein.

388 Indeed, we found that an ADAM10/Tspan15 fusion protein was expressed at the cell surface at

389 the predicted molecular weight, and was functional in a betacellulin shedding assay in a manner

390 that was comparable to when the two proteins were expressed individually. In this shedding

391 assay in the HEK-293T cell line, betacellulin shedding was entirely dependent on ADAM10, as

24

392   was previously reported in MEFs (Sahin *et al.* 2004). Our ADAM10/Tspan15 fusion protein is
393   the first example of physically linking a tetraspanin to its partner protein, as a means of
394   demonstrating that the two proteins can function as a complex. This approach may be useful for
395   the investigation of other tetraspanins and their partners. Moreover, it may facilitate attempts to
396   generate the first high-resolution structure of a tetraspanin/partner protein complex, which could
397   provide fundamental new insights comparable to the recently-reported first crystal structure of a
398   tetraspanin (Zimmerman *et al.* 2016). To date, the only structural study on a tetraspanin with its
399   partner is the relatively low resolution (6 Å) cryo-electron microscopy study of tetraspanin
400   uroplakins Ia and Ib with their uroplakin partners II and IIIa (Min *et al.* 2006).

401   Our study represents the first use of BiFC to enable the fluorescent imaging of a tetraspanin with
402   its partner. BiFC uses two fusion proteins containing each half of a fluorescent protein, such as
403   GFP, linked to the two proteins of interest, in this case ADAM10 and Tspan15. If the two
404   proteins interact, the two halves of GFP will fold to form a fluorescent GFP molecule, and
405   therefore any fluorescent signal can only be the result of a successful ADAM10/Tspan15
406   heterodimer. Consistent with the idea that ADAM10 and Tspan15 exist as a functional complex,
407   ADAM10/Tspan15 BiFC dimers were formed and localised predominantly to the plasma
408   membrane, similar to the localisation of Tspan15 itself. To investigate the dynamics of
409   ADAM10/Tspan15 dimers for the first time in living cells, FCS was used to investigate its
410   diffusion speed and clustering in the plasma membrane of transfected HEK-293T cells. An
411   average diffusion co-efficient of 0.19 μm^2/s was similar to that previously reported for ADAM10
412   (0.10 μm^2/s) on Tspan15-transfected U2OS cells (Jouannet *et al.* 2016). However, that study
413   measured ADAM10 rather than ADAM10/Tspan15 dimers (Jouannet *et al.* 2016), therefore a
414   proportion of the diffusion speed will have been contributed by other ADAM10/TspanC8
415   complexes. We also used FCS to assess the molecular brightness of ADAM10/Tspan15 BiFC
416   dimers, to estimate the degree of clustering. The existence of some traces containing a brighter
417   Tspan15/ADAM10 component was indicative of larger cluster formation, as has been observed
418   for TspanC8s and other tetraspanins by super-resolution microscopy (Zuidscherwoude *et al.*
419   2015; Marjon *et al.* 2016; Dahmane *et al.* 2019). We propose that FCS imaging of BiFC dimers
420   will be useful for the study of other tetraspanin/partner protein complexes.

421   One prediction of the idea that ADAM10 and Tspan15 exist as a heterodimeric complex is that
422   ADAM10 would be the major Tspan15-interacting partner. Using mass spectrometry to identify
423   proteins in Tspan15 immunoprecipitates from HEK-293T cells lysed in the relatively stringent
424   1% digitonin, ADAM10 was strikingly the most abundant protein. Indeed, ADAM10 was
425   almost 400 times more abundant in Tspan15 immunoprecipitates from wild-type cells versus
426   control Tspan15-knockout cells, and the only other protein identified above the false discovery
427   rate threshold was Tspan15 itself. These data are consistent with two previous studies in which
428   GFP-tagged Tspan15 was expressed in U2OS or HepG2 cells, which were lysed in relatively
429   non-stringent 1% Brij97 and Tspan15 immunoprecipitated via the GFP tag (Jouannet *et al.* 2016;
430   Sidahmed-Adrar *et al.* 2019). For example, mass spectrometry identified ADAM10 as 15-fold

25

431   more abundant than any other Tspan15-interacting proteins (Jouannet *et al.* 2016). However,

432   interpretation was complicated in these two studies because of the use of less stringent detergent

433   and the resulting large number of tetraspanin-associated proteins identified, the majority of

434   which are likely to be indirectly associated with Tspan15. In our study ,in addition to ADAM10,

435   26 proteins were identified as being significantly more detected in wild-type versus Tspan15-

436   knockout samples, but the most differential of these was only four-fold higher in wild-type.

437   Thus, it remains to be determined whether any of these are definitive ADAM10/Tspan15-

438   interacting proteins that impact functionally on the complex. Of note, we did not identify beta-

439   transducin repeat containing E3 ubiquitin protein ligase (BTRC) amongst the putative Tspan15-

440   interacting proteins. BTRC was recently reported to co-immunoprecipitate with Tspan15 from

441   lysates of oesophageal squamous cell carcinoma cell lines, and was implicated in promotion of

442   metastasis by Tspan15 via the NF-κB pathway (Zhang *et al.* 2018). The Human Protein Atlas

443   (www.proteinatlas.org) indicates that BTRC mRNA has a broad expression profile in cell lines,

444   including HEK-293T (Thul *et al.* 2017), suggesting that we should have identified BTRC if it is

445   a *bone fide* Tspan15-interacting protein. The findings of our study lead us to speculate that

446   Tspan15 may be promoting cancer via ADAM10, most likely due to cleaving of specific

447   substrates that enhance the cancer phenotype. Interestingly, gene expression data suggests that

448   Tspan15 is strongly upregulated in cholangiocarcinoma and pancreatic adenocarcinoma (Tang *et*

449   *al.* 2019), and is a marker of poor prognosis in pancreatic, renal and liver cancer (Uhlen *et al.*

450   2017). Moreover, Tspan15 has been recently implicated in oral squamous cell carcinoma

451   (Hiroshima *et al.* 2019) and hepatocellular carcinoma (Sidahmed-Adrar *et al.* 2019).

452   The generation of mAbs to certain tetraspanins is a recognised difficulty in the tetraspanin field;

453   there are no mAbs to many of the 33 human tetraspanins. To initiate this study, we generated the

454   first Tspan15 mAbs using a novel strategy. Mice were immunised with ADAM10-knockout

455   MEFs stably over-expressing human Tspan15, with the aim of focussing the mAb response on

456   Tspan15 and preventing the larger ADAM10 from masking epitopes or preventing mAb binding

457   by steric hindrance. Screening of hybridomas yielded four mouse anti-human Tspan15 mAbs,

458   each recognising a similar epitope on the large extracellular loop of Tspan15. However, the

459   importance of using ADAM10-knockout cells as the immunogen remains unclear. The

460   immunisation and hybridoma generation was outsourced to Abpro, whose proprietary mouse

461   may have contributed to the success of our approach. Furthermore, Tspan15 may be a relatively

462   easy target, since eight of the 121 amino acids in the large extracellular loop are different

463   between human and mouse, yielding 93% identity and the likelihood of distinct epitopes for

464   mAb recognition. Most other TspanC8s are more conserved between human and mouse, with

465   identities of 100, 77, 98, 96 and 97% for Tspan5, 10, 14, 17 and 33, respectively. A recent study

466   overcame the problem of the identical human and mouse Tspan5 protein sequences by

467   generating Tspan5 mAbs from Tspan5-knockout mice immunised with GFP-Tspan5-transfected

468   cells and immunoprecipitates (Saint-Pol *et al.* 2017). Nevertheless, we hypothesise that our new

469   method of using tetraspanin-transfected cells, with the tetraspanin partner(s) deleted, may be an

470   effective strategy for future tetraspanin mAb generation.

26

471   To conclude, our findings strongly suggest that Tspan15 exists as an ADAM10/Tspan15 scissor

472   complex, which may be a general theme for the other five TspanC8s. We therefore propose that

473   ADAM10 be studied in the context of its associated TspanC8. This has implications for future

474   work that should aim to determine how ADAM10/TspanC8 complexes are triggered to cleave

475   specific substrates, and whether ADAM10/TspanC8 complexes can be therapeutically targeted to

476   treat human disease.

477

478 **MATERIALS AND METHODS**

479 **Antibodies**

480 Primary antibodies were rabbit anti-FLAG (Sigma-Aldrich, Poole, UK), mouse or rabbit anti-α-
481 tubulin (Cell Signaling Technology, London, UK), mouse anti-human ADAM10 11G2 (Arduise
482 *et al.* 2008), mouse anti-Tspan5 TS52 (Saint-Pol *et al.* 2017) and negative control mouse IgG1
483 MOPC-21 (MP Biomedicals, Santa Ana, CA).

484 **Expression constructs**

485 pLVX-EF1α-IRES-Puro FLAG-tagged human Tspan15 was generated by subcloning the FLAG-
486 Tspan15 sequence into the pLVX-EF1α-IRES-Puro lentiviral plasmid (Clontech, Mountain
487 View, CA). N-terminal FLAG-tagged human and mouse TspanC8s in the pEF6-*myc*-His
488 plasmid (Invitrogen, Carlsbad, CA) were as described (Haining *et al.* 2012). A series of
489 human/mouse Tspan15 chimeric constructs were generated using a two-step PCR method to
490 incorporate mouse residues into the human Tspan15 large extracellular loop and *vice versa*.
491 GFP-tagged human Tspan5/Tspan15 chimeras in the pEGFP-N1 plasmid were as described
492 (Saint-Pol *et al.* 2017). Human Tspan15 tagged at the C-terminus with the N-terminal half of
493 superfolder GFP was generated by subcloning human Tspan15 into a pcDNA3.1/zeo split
494 superfolder GFP vector (Kilpatrick *et al.* 2012). Mouse ADAM10 tagged at the C-terminus with
495 the C-terminal half of superfolder GFP was generated using a two-step PCR approach in which
496 the GFP tag was subcloned into pcDNA3.1 mouse ADAM10 (Maretzky *et al.* 2005). pRK5M
497 human ADAM10 was a gift from Rik Derynck (Addgene plasmid # 31717) (Liu *et al.* 2009).
498 The pRK5M ADAM10-Tspan15 fusion construct was generated by subcloning human Tspan15
499 into pRK5M human ADAM10, at the C-terminus of ADAM10 to replace the myc tag. The
500 alkaline phosphatase-tagged human betacellulin construct was kindly provided by Shigeki
501 Higashiyama and Carl Blobel (Sahin *et al.* 2004).

502 **Cell culture and transfections**

503 ADAM10-knockout mouse embryonic fibroblasts (MEFs) (Reiss *et al.* 2005), human embryonic
504 kidney (HEK)-293T (HEK-293 cells expressing the large T-antigen of simian virus 40) and the
505 human lung epithelial cell line A549 were cultured in DMEM (Sigma-Aldrich), and the human T
506 cell line Jurkat was cultured in RPMI 1640 (Sigma-Aldrich), each supplemented with 10% fetal
507 bovine serum (Thermo Fisher Scientific, Loughborough, UK), 4 mM L-glutamine,100 units/ml
508 penicillin and 100 μg/ml streptomycin (Sigma-Aldrich). Human umbilical vein endothelial cells
509 (HUVECs) were isolated from umbilical cords obtained with consent from the Human
510 Biomaterials Resource Centre at the University of Birmingham, UK, and cultured in M199
511 supplemented with 10% fetal bovine serum, 4 mM glutamine, 90 μg/ml heparin (Sigma-Aldrich)
512 and bovine brain extract (Wilson *et al.* 2014), and used between passages 3 and 6. HEK-293T
513 cells were transfected using polyethyleneimine as described (Ehrhardt *et al.* 2006). A549 cells
514 were transfected with Lipofectamine 2000 (Thermo Fisher Scientific). Jurkat cells were

28

515 transfected by electroporation as previously described (Tomlinson *et al.* 2007). For siRNA
516 knockdowns, HUVECs were transfected with 10 nM Silencer Select siRNA duplexes (Thermo
517 Fisher Scientific) using Lipofectamine RNAiMAX (Thermo Fisher Scientific).

Generation of CRISPR/Cas9-knockout cell lines

519 Two guide RNA sequences were selected for each of human ADAM10 and Tspan15 using the
520 Wellcome Trust Sanger Institute's CRISPR Finder tool (Hodgkins *et al.* 2015). The following
521 primer pairs were used to encode these sequences: ADAM10 guide 1 (5'-
522 CACCGCGTCTAGATTTCCATGCCCA-3' and 5'-AAACTGGGCATGGAAATCTAGACGC-
523 3'); ADAM10 guide 2 (5'-CACCGATACCTCTCATATTTACAC-3' and 5'-
524 AAACGTGTAAATATGAGAGGTATC-3'); Tspan15 guide 1 (5'-
525 CACCGGCGCGCGCTTCTCCTACCTC-3' and 5'-AAACGAGGTAGGAGAAGCGCGCGCC-
526 3'); Tspan15 guide 2 (5'-CACCGAGCGCCCAGGATGCCGCGCG-3' and 5'-
527 AAACCGCGCGGCATCCTGGGCGCTC-3'). Each primer pair was annealed and cloned into
528 the pSpCas9 (BB)-2A-Puro (PX459) plasmid (a gift from Feng Zhang, Addgene plasmid
529 #62988) (Ran *et al.* 2013). Cells were transfected with either of the guide constructs, clonal
530 transfectants selected using 1, 2.5 and 0.5 μg/ml puromycin (Thermo Fisher Scientific) for A549,
531 HEK-293T and Jurkat cells, respectively, and knockouts confirmed by flow cytometry.

Human platelet preparation

533 Washed human platelets were isolated from whole blood by centrifugation as described
534 previously (McCarty *et al.* 2006). Blood samples were taken with consent from healthy donors.

Generation of new Tspan15 mAbs

536 To create the immunogen for mouse anti-human Tspan15 mAb generation, ADAM10-knockout
537 MEFs were transduced with lentivirus packaged with FLAG-tagged human Tspan15, produced
538 in HEK-293T cells using a previously described protocol (Reyat *et al.* 2017). Clonal cells stably
539 overexpressing Tspan15 were selected with 1 μg/ml puromycin and validated by anti-FLAG
540 western blotting. Immunisation of mice and generation of hybridomas were outsourced to Abpro
541 Therapeutics (Boston, MA).

Antibody conjugation

543 Purified Tspan15 mAbs were concentrated to 1 mg/ml using Amicon Ultra Centrifugal Filters
544 (Merck, Watford, UK) and conjugated to Alexa Fluor® 647 fluorophore with a succinimidyl
545 ester reactive dye (Thermo Fisher Scientific) at an antibody-to-dye mass ratio of 10:1 for one
546 hour at room temperature. Excess unbound dye was removed using Zeba Spin Desalting
547 Columns (Thermo Fisher Scientific). The concentration and degree of labelling of the
548 conjugated mAbs were measured spectrophotometrically.

Flow cytometry

550    $2.5–5 \times 10^5$ cells were stained with primary antibodies at 10 µg/ml, followed by fluorescein

551   isothiocyanate (FITC)-conjugated sheep anti-mouse (Sigma-Aldrich) or allophycocyanin (APC)-

552   conjugated goat anti-mouse (Thermo Fisher Scientific) secondary antibodies. Samples were

553   analysed on a FACSCalibur flow cytometer (BD Biosciences, Oxford, UK). Surface staining

554   was quantitated by its geometric mean fluorescence intensity and presented as a ratio to the

555   isotype control.

556   **Antibody binding competition assay**

557   A549 cells were incubated with 10 µg/ml MOPC-21 or Tspan15 mAbs 1C12, 4A4, 5D4 or 5F4

558   for 30 minutes on ice. The cells were then stained with 10 µg/ml of each of the Alexa Fluor®

559   647-conjugated Tspan15 mAbs for 30 minutes on ice. Relative antibody binding was analysed

560   by flow cytometry.

561   **Immunoprecipitation and western blotting**

562   Immunoprecipitation and western blotting were performed as previously described (Noy *et al.*

563   2016). Western blotting used IRDye 680RD or 800CW-conjugated secondary antibodies (LI-

564   COR Biosciences, Cambridge, UK) and an Odyssey Quantitative Infrared Imaging System (LI-

565   COR Biosciences).

566   **Sample preparation for mass spectrometry**

567   2×10^8 wild-type or Tspan15-knockout HEK-293T cells were lysed in 1% digitonin lysis buffer

568   containing protease inhibitor cocktail (Sigma-Aldrich). Lysates were pre-cleared with protein G

569   sepharose prior to immunoprecipitation with Tspan15 mAb 1C12 chemically cross-linked to

570   protein G sepharose with dimethyl pimelimidate (Thermo Fisher Scientific). Five independent

571   immunoprecipitations were carried out for each cell type. Immunoprecipitation samples in non-

572   reducing Laemmli buffer were subjected to a modified single-pot solid-phase-enhanced sample

573   preparation (SP3) protocol (Hughes *et al.* 2019). Briefly, 10 µl of a 4 µg/µl bead slurry of Sera-

574   Mag SpeedBeads A and B (GE Healthcare, Chicago, IL) were added to the samples. Protein

575   binding to the magnetic beads was achieved by adding acetonitrile to a final volume of 70% (v/v)

576   and mixing at 1200 rpm at 24 °C for 30 minutes in a Thermomixer (Eppendorf, Hamburg,

577   Germany). Magnetic beads were retained in a DynaMag-2 magnetic rack (Thermo Fisher

578   Scientific) and the supernatant was discarded. Disulfide bridges were reduced by adding 20 µl of

579   30 mM dithiothreitol (Biozol, Eching, Germany) and incubating at 1200 rpm at 37 °C for 30

580   minutes. Cysteines were alkylated by adding 25 µl of 80 mM iodoactemamide (Sigma-Aldrich)

581   and incubating at 1200 rpm at 24 °C for 30 minutes in the dark in a Thermomixer. The reaction

582   was quenched by adding 3 µl of 200 mM dithiothreitol. Protein binding to the beads was

583   repeated in 70% (v/v) acetonitrile for 30 minutes. After removing the solvent, beads were

584   washed twice in 200 µl 70% (v/v) ethanol and twice in 180 µl of 100% (v/v) acetonitrile. Next,

585   250 ng of LysC and 250 ng of trypsin (Promega, Mannheim, Germany) were added in 20 µl of

586   50 mM ammonium bicarbonate (Sigma Aldrich). The protein digestion was performed for 16

587   hours at room temperature. Samples were acidified with formic acid to a final concentration of
588   1% (v/v) and placed in a magnetic rack. The supernatants were transferred into fresh 0.5 ml
589   protein LoBind tubes (Eppendorf). A volume of 20 µl of 2% (v/v) dimethyl sulfoxide was added
590   to the beads and subjected to sonication for 30 seconds in a water bath. Tubes were placed in the
591   magnetic rack and the supernatants were transferred. The samples were dried in a vacuum
592   centrifuge and dissolved in 20 µl 0.1% formic acid.

Liquid chromatography coupled with tandem mass spectrometry (LC-MS/MS) analysis

594   Samples were analyzed by LC-MS/MS for relative label free protein quantification. A volume
595   of 10 µl per sample was separated on a nanoLC system (EASY-nLC 1200, Thermo Fisher
596   Scientific) using an in-house packed C18 column (30 cm x 75 µm ID, ReproSil-Pur 120 C18-
597   AQ, 1.9 µm; Dr. Maisch GmbH, Ammerbuch, Germany) with a binary gradient of water (A) and
598   acetonitrile (B) containing 0.1% formic acid at 50 °C column temperature and a flow rate of 250
599   nl/minute (gradient: 0 minutes 2.4% B; 2 minutes, 4.8% B; 92 minutes, 24% B; 112 minutes,
600   35.2% B; 121 minutes, 60% B).

601   The nanoLC was coupled online via a nanospray flex ion source (Proxeon, Thermo Fisher
602   Scientific) equipped with a PRSO-V2 column oven (Sonation, Biberach an der Riss, Germany)
603   to a Q-Exactive HF mass spectrometer (Thermo Fisher Scientific). Full MS spectra were
604   acquired at a resolution of 120,000. The top 15 peptide ions were chosen for Higher-energy C-
605   trap Dissociation (HCD) (normalized collision energy of 26%, automatic gain control 1E+5 ions,
606   intensity threshold 5E+3 ions, maximum ion trapping time 100 ms). Fragment ion spectra were
607   acquired at a resolution of 15,000. A dynamic exclusion of 120 s was used for peptide
608   fragmentation.

Data analysis and label free quantification

610   The raw data was analyzed by Maxquant software (maxquant.org, Max-Planck Institute Munich)
611   version 1.6.6.0 (Cox *et al.* 2014). The MS data was searched against a fasta database of *Homo*
612   *sapiens* from UniProt (download: June 12th 2019, 20962 entries). Trypsin was defined as the
613   protease. Two missed cleavages were allowed for the database search. The option first search
614   was used to recalibrate the peptide masses within a window of 20 ppm. For the main search,
615   peptide and peptide fragment mass tolerances were set to 4.5 and 20 ppm, respectively.
616   Carbamidomethylation of cysteine was defined as static modification. Acetylation of the protein
617   N-terminus and oxidation of methionine were set as variable modifications. The false discovery
618   rate for both peptides and proteins was adjusted to less than 1%. Label free quantification of
619   proteins required at least two ratio counts of unique peptides. Only unique peptides were used
620   for quantification. The option "match between runs" was enabled with a matching time of 1
621   minute.

622   The protein label free quantification intensities were log$_2$ transformed and a two-sided Student's
623   *t*-test was applied to evaluate the significance of proteins with changed abundance between the

624 TSPAN15 immunoprecipitation from wild-type samples and the control immunoprecipitation
625 from Tspan15-knockout samples. Additionally, a permutation-based false discovery rate
626 estimation was used (Tusher *et al.* 2001).

Quantitative reverse-transcription PCR (qRT-PCR)

628 RNA was extracted using the RNeasy Mini kit (Qiagen, Manchester, UK) from cells
629 homogenised with QIAshredder columns (Qiagen). Complementary DNA was generated using
630 the High Capacity cDNA Reverse Transcription kit (Thermo Fisher Scientific) and subjected to
631 TaqMan qPCR assays (Thermo Fisher Scientific) for Tspan15 (Hs00202548_m1) and GAPDH
632 (Hs02758991_g1) and analysed as described (Reyat *et al.* 2017). All qPCR data were
633 normalised to GAPDH as the internal loading control.

Confocal microscopy

635 All reagents are from Sigma-Aldrich unless otherwise stated. Cells were fixed with 10%
636 formalin for 15 minutes and washed three times with PBS (0.01 M phosphate, 0.0027 M KCl,
637 0.137 M NaCl, pH 7.4) before blocking in PBS containing 1% BSA, 2% goat serum (or mouse
638 serum for direct staining with conjugated mouse primary antibodies) and 0.1% saponin for 20
639 minutes to permeabilise the cells. The same buffer was used for antibody dilutions. Cells were
640 incubated with antibodies for one hour and washed three to four times with PBS after
641 incubations. For direct labelling of Tspan15, cells were stained with 5 µg/ml Alexa Fluor® 647-
642 conjugated Tspan15 mAb (5D4). For simultaneous staining of ADAM10 and Tspan15, cells
643 were first stained with 0.5 µg/ml ADAM10 mAb (11G2) and then secondarily labelled with
644 Alexa Fluor®-conjugated goat anti-mouse antibody, followed by direct staining of Tspan15 as
645 described above. Confocal Z-stacks of stained cells were taken at 1 µm intervals on a Leica TCS
646 SP2 confocal microscope (Leica Biosystems, Wetzlar, Germany) with 488 nm Argon and 633
647 nm Helium/Neon laser lines with a 63x 1.4 NA oil objective. For imaging of non-permeabilised
648 cells, the Nikon A1R confocal system (Nikon, Tokyo, Japan), equipped with a 100x 1.4 NA oil
649 objective and similar lasers to those above, was used for acquisition of z-stacks.

Fluorescence correlation spectroscopy (FCS)

651 1.5×10^4 HEK-293T cells were seeded onto Nunc Lab-Tek 8-well glass-bottomed chamber
652 slides (0.13-0.17 mm thick, #1.0 borosilicate glass) (Thermo Fisher Scientific) pre-coated with
653 10 µg/ml poly-D-lysine (Sigma-Aldrich). 24 hours later, cells were transfected with ADAM10
654 and Tspan15 split superfolder GFP (sfGFP) expression constructs. After a further 24 hours,
655 media was replaced with 200 µl/well HEPES-buffered saline solution (2 mM sodium pyruvate,
656 145 mM NaCl, 10 mM D-glucose, 5 mM KCl, 1 mM $MgSO_4.7H_2O$, 10 mM HEPES, 1.3 mM
657 $CaCl_2$, 1.5 mM $NaHCO_3$, pH 7.45) and equilibrated for 10 minutes at 22 °C prior to FCS
658 recording on a Zeiss LSM 510NLO Confocor 3 microscope (Carl Zeiss, Jena, Germany).
659 Fluorescence fluctuations were collected using a c-Apochromat 40x 1.2 NA water immersion
660 objective using 488 nm excitation with emission collected through a 505-600 long pass filter.

661 FCS acquisition, autocorrelation and photon counting histogram (PCH) analyses were performed
662 as described previously (Ayling *et al.* 2012). In brief, the confocal volume was calibrated with
663 20 nM rhodamine 6G dye on each experimental day. For cell measurements, the detection
664 volume was positioned in x-y over the cell of interest using a live confocal image, and then on
665 the apical cell membrane following a z-intensity scan using ~0.04 kW/cm^2 laser power.
666 Fluctuation traces were recorded at 22 °C on the apical membrane for each cell for 30 seconds
667 using ~0.17 kW/cm^2 laser power. Autocorrelation and PCH analyses were performed in Zen
668 2012 (Carl Zeiss), with the first 5 seconds of fluctuations routinely removed to adjust for
669 photobleaching. Autocorrelation curves were fitted to a two-component, 2D diffusion model
670 with a pre-exponential term to account for sfGFP blinking, with an offset added where necessary
671 to obtain average dwell times and particle numbers. As previously demonstrated, component 1
672 (300-600 μs) represents a dark state of the sfGFP fluorophore, whilst component 2 represents the
673 dwell time of the sfGFP-labelled complex (Ayling *et al.* 2012; Kilpatrick *et al.* 2012). Diffusion
674 coefficients of the sfGFP-labelled complex were calculated for each trace using the equation $D =$
675 $\omega_0^2/4.\tau_D$, where ω_0 is the radius of the detection volume (obtained from calibration) and τ_D the
676 average dwell time of component 2. Particle numbers of component 2 were expressed as
677 particles per μm^2, calculated from $N = N(\tau_{D2})/\pi.\omega_0^2$, where $N(\tau_{D2})$ is the fractional contribution
678 of component 2 to the total particle number determined from the autocorrelation curve.
679 Molecular brightness of complexes was determined using PCH analyses carried out on the same
680 fluctuation traces as used for autocorrelation analyses using Zen 2012. Traces were binned at
681 100 μs and fitted to either a 1- or 2-component PCH model with the first order correction fixed at
682 0.3, as determined from the calibration read. Data are shown as values obtained from individual
683 cell membranes, obtained over 'n' independent transfections.

Betacellulin shedding assay

685 ADAM10/Tspan15 double knockout HEK-293T cells were transfected in 24-well plates with
686 200 ng of alkaline phosphatase-conjugated betacellulin expression construct and 50 ng total of
687 ADAM10, Tspan15, ADAM10 plus Tspan15, or the ADAM10/Tspan15 fusion construct. 24
688 hours post transfection, cells were washed and stimulated with 2 mM N-ethylmaleimide (NEM)
689 (Sigma-Aldrich), or ethanol vehicle control, for 2.5 hours in Opti-MEM reduced serum media
690 (Thermo Fisher Scientific). Alkaline phosphatase activity in supernatant and cell lysate samples
691 were measured using p-nitrophenyl phosphate (pNPP) substrate (Sigma-Aldrich) and a VICTOR
692 X3 Multilabel Plate Reader (Perkin Elmer, Seer Green, UK). The supernatant activity as a
693 percentage of the total was calculated to determine the percentage shedding.

Statistical analyses

695 Relative data were normalised by either log- or arscine-transformation before being statistical
696 analysed using ANOVA with post-hoc multiple comparison tests, as indicated in the figure
697 legends.

33

698 **ACKNOWLEDGMENTS**

711

712

713 **COMPETING INTERESTS**

714 The authors declare no competing interests.

715

716 **REFERENCES**

717 Arduise, C., T. Abache, L. Li, M. Billard, A. Chabanon, A. Ludwig, P. Mauduit, C. Boucheix, E.
718 Rubinstein and F. Le Naour (2008). Tetraspanins regulate ADAM10-mediated cleavage of TNF-
719 alpha and epidermal growth factor. *J Immunol* **181**: 7002-7013.

720 Ayling, L. J., S. J. Briddon, M. L. Halls, G. R. Hammond, L. Vaca, J. Pacheco, S. J. Hill and D.
721 M. Cooper (2012). Adenylyl cyclase AC8 directly controls its micro-environment by recruiting
722 the actin cytoskeleton in a cholesterol-rich milieu. *J Cell Sci* **125**: 869-886. 10.1242/jcs.091090.

723 Brummer, T., S. A. Muller, F. Pan-Montojo, F. Yoshida, A. Fellgiebel, T. Tomita, K. Endres and
724 S. F. Lichtenthaler (2019). NrCAM is a marker for substrate-selective activation of ADAM10 in
725 Alzheimer's disease. *EMBO Mol Med* **11**: e9695. 10.15252/emmm.201809695.

726 Brummer, T., M. Pigoni, A. Rossello, H. Wang, P. J. Noy, M. G. Tomlinson, C. P. Blobel and S.
727 F. Lichtenthaler (2018). The metalloprotease ADAM10 (a disintegrin and metalloprotease 10)
728 undergoes rapid, postlysis autocatalytic degradation. *FASEB J* **32**: 3560-3573.
729 10.1096/fj.201700823RR.

730 Cox, J., M. Y. Hein, C. A. Luber, I. Paron, N. Nagaraj and M. Mann (2014). Accurate proteome-
731 wide label-free quantification by delayed normalization and maximal peptide ratio extraction,
732 termed MaxLFQ. *Mol Cell Proteomics* **13**: 2513-2526. 10.1074/mcp.M113.031591.

733 Dahmane, S., C. Doucet, A. Le Gall, C. Chamontin, P. Dosset, F. Murcy, L. Fernandez, D. Salas,
734 E. Rubinstein, M. Mougel, M. Nollmann and P. E. Milhiet (2019). Nanoscale organization of
735 tetraspanins during HIV-1 budding by correlative dSTORM/AFM. *Nanoscale* **11**: 6036-6044.
736 10.1039/c8nr07269h.

737 Dornier, E., F. Coumailleau, J. F. Ottavi, J. Moretti, C. Boucheix, P. Mauduit, F. Schweisguth
738 and E. Rubinstein (2012). TspanC8 tetraspanins regulate ADAM10/Kuzbanian trafficking and
739 promote Notch activation in flies and mammals. *J Cell Biol* **199**: 481-496.
740 10.1083/jcb.201201133.

741 Ehrhardt, C., M. Schmolke, A. Matzke, A. Knoblauch, C. Will, V. Wixler and S. Ludwig (2006).
742 Polyethylenimine, a cost-effective transfection reagent. *Signal Transduction* **6**: 179–184.

743 Haining, E. J., J. Yang, R. L. Bailey, K. Khan, R. Collier, S. Tsai, S. P. Watson, J. Frampton, P.
744 Garcia and M. G. Tomlinson (2012). The TspanC8 subgroup of tetraspanins interacts with A
745 disintegrin and metalloprotease 10 (ADAM10) and regulates its maturation and cell surface
746 expression. *J Biol Chem* **287**: 39753-39765. 10.1074/jbc.M112.416503.

747 Hiroshima, K., M. Shiiba, N. Oka, F. Hayashi, S. Ishida, R. Fukushima, K. Koike, M. Iyoda, D.
748 Nakashima, H. Tanzawa and K. Uzawa (2019). Tspan15 plays a crucial role in metastasis in oral
749 squamous cell carcinoma. *Exp Cell Res*: 111622. 10.1016/j.yexcr.2019.111622.

750 Hodgkins, A., A. Farne, S. Perera, T. Grego, D. J. Parry-Smith, W. C. Skarnes and V. Iyer
751 (2015). WGE: a CRISPR database for genome engineering. *Bioinformatics* **31**: 3078-3080.
752 10.1093/bioinformatics/btv308.

753   Hughes, C. S., S. Moggridge, T. Muller, P. H. Sorensen, G. B. Morin and J. Krijgsveld (2019).
754   Single-pot, solid-phase-enhanced sample preparation for proteomics experiments. *Nat Protoc* **14**:
755   68-85. 10.1038/s41596-018-0082-x.

756   Jouannet, S., J. Saint-Pol, L. Fernandez, V. Nguyen, S. Charrin, C. Boucheix, C. Brou, P. E.
757   Milhiet and E. Rubinstein (2016). TspanC8 tetraspanins differentially regulate the cleavage of
758   ADAM10 substrates, Notch activation and ADAM10 membrane compartmentalization. *Cell Mol*
759   *Life Sci* **73**: 1895-1915. 10.1007/s00018-015-2111-z.

760   Kilpatrick, L. E., S. J. Briddon and N. D. Holliday (2012). Fluorescence correlation
761   spectroscopy, combined with bimolecular fluorescence complementation, reveals the effects of
762   beta-arrestin complexes and endocytic targeting on the membrane mobility of neuropeptide Y
763   receptors. *Biochim Biophys Acta* **1823**: 1068-1081. 10.1016/j.bbamcr.2012.03.002.

764   Lichtenthaler, S. F., M. K. Lemberg and R. Fluhrer (2018). Proteolytic ectodomain shedding of
765   membrane proteins in mammals-hardware, concepts, and recent developments. *EMBO J* **37**.
766   10.15252/embj.201899456.

767   Liu, C., P. Xu, S. Lamouille, J. Xu and R. Derynck (2009). TACE-mediated ectodomain
768   shedding of the type I TGF-beta receptor downregulates TGF-beta signaling. *Mol Cell* **35**: 26-36.
769   10.1016/j.molcel.2009.06.018.

770   Maretzky, T., M. Schulte, A. Ludwig, S. Rose-John, C. Blobel, D. Hartmann, P. Altevogt, P.
771   Saftig and K. Reiss (2005). L1 is sequentially processed by two differently activated
772   metalloproteases and presenilin/gamma-secretase and regulates neural cell adhesion, cell
773   migration, and neurite outgrowth. *Mol Cell Biol* **25**: 9040-9053. 10.1128/MCB.25.20.9040-
774   9053.2005.

775   Marjon, K. D., C. M. Termini, K. L. Karlen, C. Saito-Reis, C. E. Soria, K. A. Lidke and J. M.
776   Gillette (2016). Tetraspanin CD82 regulates bone marrow homing of acute myeloid leukemia by
777   modulating the molecular organization of N-cadherin. *Oncogene* **35**: 4132-4140.
778   10.1038/onc.2015.449.

779   Matthews, A. L., C. Z. Koo, J. Szyroka, N. Harrison, A. Kanhere and M. G. Tomlinson (2018).
780   Regulation of Leukocytes by TspanC8 Tetraspanins and the "Molecular Scissor" ADAM10.
781   *Front Immunol* **9**: 1451. 10.3389/fimmu.2018.01451.

782   Matthews, A. L., P. J. Noy, J. S. Reyat and M. G. Tomlinson (2017). Regulation of A disintegrin
783   and metalloproteinase (ADAM) family sheddases ADAM10 and ADAM17: The emerging role
784   of tetraspanins and rhomboids. *Platelets* **28**: 333-341. 10.1080/09537104.2016.1184751.

785   Matthews, A. L., J. Szyroka, R. Collier, P. J. Noy and M. G. Tomlinson (2017). Scissor sisters:
786   regulation of ADAM10 by the TspanC8 tetraspanins. *Biochem Soc Trans* **45**: 719-730.
787   10.1042/BST20160290.

788   McCarty, O. J., S. D. Calaminus, M. C. Berndt, L. M. Machesky and S. P. Watson (2006). von
789   Willebrand factor mediates platelet spreading through glycoprotein Ib and alpha(IIb)beta3 in the
790   presence of botrocetin and ristocetin, respectively. *J Thromb Haemost* **4**: 1367-1378.

791   Min, G., H. Wang, T. T. Sun and X. P. Kong (2006). Structural basis for tetraspanin functions as
792   revealed by the cryo-EM structure of uroplakin complexes at 6-A resolution. *J Cell Biol* **173**:
793   975-983.

794   Noy, P. J., J. Yang, J. S. Reyat, A. L. Matthews, A. E. Charlton, J. Furmston, D. A. Rogers, G. E.
795   Rainger and M. G. Tomlinson (2016). TspanC8 Tetraspanins and A Disintegrin and
796   Metalloprotease 10 (ADAM10) Interact via Their Extracellular Regions: EVIDENCE FOR
797   DISTINCT BINDING MECHANISMS FOR DIFFERENT TspanC8 PROTEINS. *J Biol Chem*
798   **291**: 3145-3157. 10.1074/jbc.M115.703058.

799   Prox, J., M. Willenbrock, S. Weber, T. Lehmann, D. Schmidt-Arras, R. Schwanbeck, P. Saftig
800   and M. Schwake (2012). Tetraspanin15 regulates cellular trafficking and activity of the
801   ectodomain sheddase ADAM10. *Cell Mol Life Sci* **69**: 2919-2932. 10.1007/s00018-012-0960-2.

802   Ran, F. A., P. D. Hsu, J. Wright, V. Agarwala, D. A. Scott and F. Zhang (2013). Genome
803   engineering using the CRISPR-Cas9 system. *Nat Protoc* **8**: 2281-2308. 10.1038/nprot.2013.143.

804   Reiss, K., T. Maretzky, A. Ludwig, T. Tousseyn, B. de Strooper, D. Hartmann and P. Saftig
805   (2005). ADAM10 cleavage of N-cadherin and regulation of cell-cell adhesion and beta-catenin
806   nuclear signalling. *EMBO J* **24**: 742-752. 10.1038/sj.emboj.7600548.

807   Reyat, J. S., M. Chimen, P. J. Noy, J. Szyroka, G. E. Rainger and M. G. Tomlinson (2017).
808   ADAM10-Interacting Tetraspanins Tspan5 and Tspan17 Regulate VE-Cadherin Expression and
809   Promote T Lymphocyte Transmigration. *J Immunol* **199**: 666-676. 10.4049/jimmunol.1600713.

810   Reyat, J. S., M. G. Tomlinson and P. J. Noy (2017). Utilizing Lentiviral Gene Transfer in
811   Primary Endothelial Cells to Assess Lymphocyte-Endothelial Interactions. *Methods Mol Biol*
812   **1591**: 155-168. 10.1007/978-1-4939-6931-9_11.

813   Rubinstein, E., S. Charrin and M. G. Tomlinson (2013). Organisation of the tetraspanin web.
814   Tetraspanins. F. Berditchevski and E. Rubinstein. Dordrecht, Springer**:** 47-90.

815   Sahin, U., G. Weskamp, K. Kelly, H. M. Zhou, S. Higashiyama, J. Peschon, D. Hartmann, P.
816   Saftig and C. P. Blobel (2004). Distinct roles for ADAM10 and ADAM17 in ectodomain
817   shedding of six EGFR ligands. *Journal of Cell Biology* **164**: 769-779.

818   Saint-Pol, J., M. Billard, E. Dornier, E. Eschenbrenner, L. Danglot, C. Boucheix, S. Charrin and
819   E. Rubinstein (2017). New insights into the tetraspanin Tspan5 using novel monoclonal
820   antibodies. *J Biol Chem* **292**: 9551-9566. 10.1074/jbc.M116.765669.

821   Saint-Pol, J., E. Eschenbrenner, E. Dornier, C. Boucheix, S. Charrin and E. Rubinstein (2017).
822   Regulation of the trafficking and the function of the metalloprotease ADAM10 by tetraspanins.
823   *Biochem Soc Trans* **45**: 937-944. 10.1042/BST20160296.

824   Seipold, L., H. Altmeppen, T. Koudelka, A. Tholey, P. Kasparek, R. Sedlacek, M. Schweizer, J.
825   Bar, M. Mikhaylova, M. Glatzel and P. Saftig (2018). In vivo regulation of the A disintegrin and
826   metalloproteinase 10 (ADAM10) by the tetraspanin 15. *Cell Mol Life Sci* **75**: 3251-3267.
827   10.1007/s00018-018-2791-2.

828   Shah, J., F. Rouaud, D. Guerrera, E. Vasileva, L. M. Popov, W. L. Kelley, E. Rubinstein, J. E.
829   Carette, M. R. Amieva and S. Citi (2018). A Dock-and-Lock Mechanism Clusters ADAM10 at

830   Cell-Cell Junctions to Promote alpha-Toxin Cytotoxicity. *Cell Rep* **25**: 2132-2147 e2137.
831   10.1016/j.celrep.2018.10.088.

832   Sidahmed-Adrar, N., J. F. Ottavi, N. Benzoubir, T. Ait Saadi, M. Bou Saleh, P. Mauduit, C.
833   Guettier, C. Desterke and F. Le Naour (2019). Tspan15 Is a New Stemness-Related Marker in
834   Hepatocellular Carcinoma. *Proteomics*: e1900025. 10.1002/pmic.201900025.

835   Sievers, F., A. Wilm, D. Dineen, T. J. Gibson, K. Karplus, W. Li, R. Lopez, H. McWilliam, M.
836   Remmert, J. Soding, J. D. Thompson and D. G. Higgins (2011). Fast, scalable generation of
837   high-quality protein multiple sequence alignments using Clustal Omega. *Mol Syst Biol* **7**: 539.
838   10.1038/msb.2011.75.

839   Tang, Z., B. Kang, C. Li, T. Chen and Z. Zhang (2019). GEPIA2: an enhanced web server for
840   large-scale expression profiling and interactive analysis. *Nucleic Acids Res* **47**: W556-W560.
841   10.1093/nar/gkz430.

842   Termini, C. M. and J. M. Gillette (2017). Tetraspanins Function as Regulators of Cellular
843   Signaling. *Front Cell Dev Biol* **5**: 34. 10.3389/fcell.2017.00034.

844   Thul, P. J., L. Akesson, M. Wiking, D. Mahdessian, A. Geladaki, H. Ait Blal, T. Alm, A.
845   Asplund, L. Bjork, L. M. Breckels, A. Backstrom, F. Danielsson, L. Fagerberg, J. Fall, L. Gatto,
846   C. Gnann, S. Hober, M. Hjelmare, F. Johansson, S. Lee, C. Lindskog, J. Mulder, C. M. Mulvey,
847   P. Nilsson, P. Oksvold, J. Rockberg, R. Schutten, J. M. Schwenk, A. Sivertsson, E. Sjostedt, M.
848   Skogs, C. Stadler, D. P. Sullivan, H. Tegel, C. Winsnes, C. Zhang, M. Zwahlen, A. Mardinoglu,
849   F. Ponten, K. von Feilitzen, K. S. Lilley, M. Uhlen and E. Lundberg (2017). A subcellular map
850   of the human proteome. *Science* **356**. 10.1126/science.aal3321.

851   Tomlinson, M. G., S. D. Calaminus, O. Berlanga, J. M. Auger, T. Bori-Sanz, L. Meyaard and S.
852   P. Watson (2007). Collagen promotes sustained glycoprotein VI signaling in platelets and cell
853   lines. *J Thromb Haemost* **5**: 2274-2283.

854   Tomlinson, M. G., T. Hanke, D. A. Hughes, A. N. Barclay, E. Scholl, T. Hünig and M. D.
855   Wright (1995). Characterization of mouse CD53: epitope mapping, cellular distribution and
856   induction by T cell receptor engagement during repertoire selection. *Eur J Immunol* **25**: 2201-
857   2206.

858   Tomlinson, M. G., A. F. Williams and M. D. Wright (1993). Epitope mapping of anti-rat CD53
859   monoclonal antibodies. Implications for the membrane orientation of the transmembrane 4
860   superfamily. *Eur J Immunol* **23**: 136-140.

861   Tusher, V. G., R. Tibshirani and G. Chu (2001). Significance analysis of microarrays applied to
862   the ionizing radiation response. *Proc Natl Acad Sci U S A* **98**: 5116-5121.
863   10.1073/pnas.091062498.

864   Uhlen, M., C. Zhang, S. Lee, E. Sjostedt, L. Fagerberg, G. Bidkhori, R. Benfeitas, M. Arif, Z.
865   Liu, F. Edfors, K. Sanli, K. von Feilitzen, P. Oksvold, E. Lundberg, S. Hober, P. Nilsson, J.
866   Mattsson, J. M. Schwenk, H. Brunnstrom, B. Glimelius, T. Sjoblom, P. H. Edqvist, D.
867   Djureinovic, P. Micke, C. Lindskog, A. Mardinoglu and F. Ponten (2017). A pathology atlas of
868   the human cancer transcriptome. *Science* **357**. 10.1126/science.aan2507.

869   van Deventer, S. J., V. E. Dunlock and A. B. van Spriel (2017). Molecular interactions shaping
870   the tetraspanin web. *Biochem Soc Trans* **45**: 741-750. 10.1042/BST20160284.

871   Virreira Winter, S., A. Zychlinsky and B. W. Bardoel (2016). Genome-wide CRISPR screen
872   reveals novel host factors required for Staphylococcus aureus alpha-hemolysin-mediated
873   toxicity. *Sci Rep* **6**: 24242. 10.1038/srep24242.

874   Wetzel, S., L. Seipold and P. Saftig (2017). The metalloproteinase ADAM10: A useful
875   therapeutic target? *Biochim Biophys Acta*. 10.1016/j.bbamcr.2017.06.005.

876   Wilson, E., K. Leszczynska, N. S. Poulter, F. Edelmann, V. A. Salisbury, P. J. Noy, A. Bacon, J.
877   Z. Rappoport, J. K. Heath, R. Bicknell and V. L. Heath (2014). RhoJ interacts with the GIT-PIX
878   complex and regulates focal adhesion disassembly. *J Cell Sci* **127**: 3039-3051.
879   10.1242/jcs.140434.

880   Zhang, B., Z. Zhang, L. Li, Y. R. Qin, H. Liu, C. Jiang, T. T. Zeng, M. Q. Li, D. Xie, Y. Li, X.
881   Y. Guan and Y. H. Zhu (2018). TSPAN15 interacts with BTRC to promote oesophageal
882   squamous cell carcinoma metastasis via activating NF-kappaB signaling. *Nat Commun* **9**: 1423.
883   10.1038/s41467-018-03716-9.

884   Zhou, J., T. Fujiwara, S. Ye, X. Li and H. Zhao (2014). Downregulation of Notch modulators,
885   tetraspanin 5 and 10, inhibits osteoclastogenesis in vitro. *Calcif Tissue Int* **95**: 209-217.
886   10.1007/s00223-014-9883-2.

887   Zimmerman, B., B. Kelly, B. J. McMillan, T. C. Seegar, R. O. Dror, A. C. Kruse and S. C.
888   Blacklow (2016). Crystal Structure of a Full-Length Human Tetraspanin Reveals a Cholesterol-
889   Binding Pocket. *Cell* **167**: 1041-1051. 10.1016/j.cell.2016.09.056.

890   Zuidscherwoude, M., F. Gottfert, V. M. Dunlock, C. G. Figdor, G. van den Bogaart and A. B.
891   van Spriel (2015). The tetraspanin web revisited by super-resolution microscopy. *Sci Rep* **5**:
892   12201. 10.1038/srep12201.

893